Herbert Venghaus
Norbert Grote *Editors*

Fibre Optic Communication

Key Devices

2nd Edition

Springer

Chapter 10
Optical Switches

Shifu Yuan and John E. Bowers

Abstract After a detailed introductory discussion of general concepts, which apply to optical switches regardless of their implementation technology, the following sections cover opto-mechanical switches and liquid crystal technologies for optical switching, including small matrix switches and wavelength selective switches. Planar lightwave circuit (PLC) based optical switch technologies constitute the topic of the next section, and the treatment includes switches in various material systems such as LiNbO$_3$, polymer, silicon-on-insulator (SOI), and switching by means of the electro-optic- or thermo-optic effect. The following, major part of the chapter covers MEMS-based switches including 2D and 3D switches, switching matrices and wavelength selective switches as well. The chapter concludes with a brief discussion of piezo-electric actuator-based matrix switches. The description of optical switches includes their fundamentals, including underlying physics, operation principles, and generic implementations, typical characteristics of commercially available devices, and recent developments of switches that are still in the R&D stage.

10.1 General Concepts of Optical Switching

10.1.1 Introduction

Optical switches are important devices for optical fiber communication systems where they are used for protection, restoration, wavelength routing, fiber-management, automatic patch panel, and in optical cross-connects [1–3]. As the majority of optical communication systems use single mode fibers (SMFs), we will focus on SMF optical switches in this chapter. An optical switch offers to optically switch fiber circuits without doing expensive optical-electronic-optical (OEO) con-

S. Yuan (✉)
Calient Technologies, 25 Castilian Drive, Goleta, CA 93117, USA
e-mail: syuan@calient.net

J.E. Bowers
Electrical and Computer Engineering Department, University of California, Santa Barbara,
CA 93106, USA
e-mail: bowers@ece.ucsb.edu

versions. Such a switch is transparent to all protocols, data formats, and modulation formats since it only rearranges the physical fiber circuit.

The various classes of optical switches include 1×2, 2×2, $1 \times N$, and large scale $N \times M$ matrix switches, wavelength selective switches (WSSs), and multi-cast $N \times M$ switches. Each category of optical switches has different technologies for implementation including liquid crystal (LC), planar lightwave circuit (PLC), micro-electro-mechanical-system (MEMS), and piezo-electronic actuator based technologies.

Most optical switches use an electronically controlled mechanism to switch an optical signal into different directions. However, there are also all-optical switches that use optical signals to control switches [4] but these are beyond the scope of the present chapter. We will also not deal with optical switches that comprise optical gain elements (e.g. optical amplifiers) designated as active optical switches [5] but we will restrict ourselves to passive optical switches, and the present chapter will be organized as follows: Sect. 10.1 discusses general concepts that apply to optical switches regardless of their implementation technology. Section 10.2 discusses opto-mechanical switches, and Sect. 10.3 covers liquid crystal technologies for optical switching, including small matrix switches and wavelength selective switches. The topic of Sect. 10.4 are planar lightwave circuit based optical switch technologies, Sect. 10.5 is devoted to MEMS-based optical switches, including 2D MEMS switches, 3D MEMS switches, and MEMS-based WSSs, and Sect. 10.6 briefly discusses piezo-electric actuator-based matrix switches.

10.1.2 Basics

The most simple, generic switching elements are 1×2 and 2×2 switches. As illustrated in Fig. 10.1, a 2×2 switch can switch between its "bar" and "cross" state, and switching may be digital or continuous, depending on implementation of the switch. An illustration of a 2×2 switch using a digital actuator is also illustrated in Fig. 10.1. 1×2 and 2×2 switches can be devices in their own right (see Sect. 10.2) and they can be cascaded resulting in larger switching matrices.

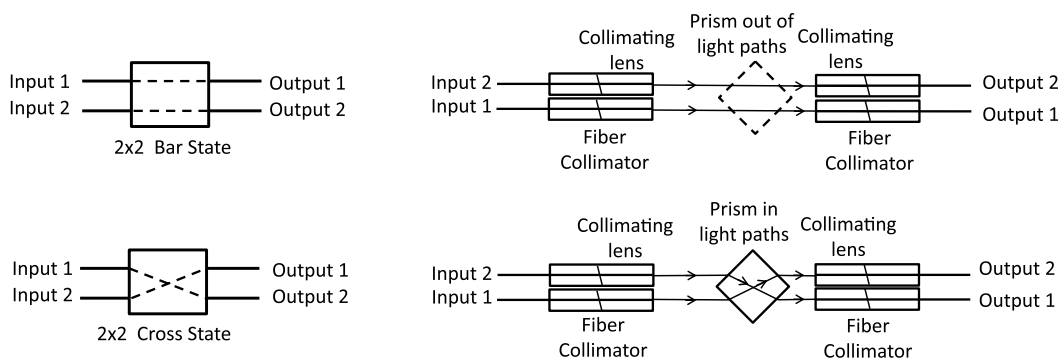**Fig. 10.1** Simple 2×2 optical switch, schematic (*left*) and mechanical switch using prism as digital actuator (*right*)

10.1.3 Optical Matrix Switches

10.1.3.1 General Aspects

An optical matrix switch [6] has input ports and output ports and the switch selectively sets up a connection between one input port i and one output port j which can be described as a pair of ports, e.g., (i, j). When a connection is (not) set up, the connection is called in the on (off) state, and it might be worthwhile to note that a port can only be used in one connection at a given instant. Optical paths are essentially bidirectional so that a signal from port i to port j can equally propagate from port j to port i. However, if a switch has optical power monitoring for feedback control, the light propagation direction is important, and with respect to monitoring, such switches may be classified as unidirectional.

An optical matrix switch can be called an $M \times N$ optical switch with M input and N output ports. Telcordia definition GR-1073 [6] does not specify which ports are input and output ports since the switch is typically bidirectional. However, in order to avoid confusion, we will consider an $M \times N$ switch to have M input and N output ports with the understanding that the signal might be bidirectional.

An optical matrix switch should meet a number of requirements including: small insertion loss, low crosstalk, fast switching time, good directivity, and small footprint. In addition, non-blocking operation may also be required or may even be mandatory [6] where "non-blocking" includes the following variants:

Strict-sense non-blocking: it is possible to establish a new path from any unused input to any unused output port, no matter what paths are set already.
Wide-sense non-blocking: after connections have already been set, it is still possible to connect any unused input to any unused output using dedicated algorithms without interrupting the connections set-up already.
Re-arrangeably non-blocking: the switch enables any connection from inputs to outputs provided all connections to be made are known in advance. If connections have been made before, disconnecting and resetting existing connections may be required in order to make the new connections.
*Blocking switch*: new connections from free input to free output ports cannot be made at all once a certain number of connections have been set.

For most telecom applications switches need to be strict-sense or wide-sense non-blocking while blocking and re-arrangeable non-blocking switches are typically not acceptable.

10.1.3.2 Optical Matrix Switch Architectures

Optical Matrix Switches Using Digital Switching Elements   Optical matrix switch architectures are essentially based upon two types of actuators: either digital actuators that switch/steer light paths digitally to the 'on' or 'off' position, or analogue actuators that enable directing optical signals to many positions

Fig. 10.2 Example of 8×8 crossbar switch using 2×2 optical switches [6]
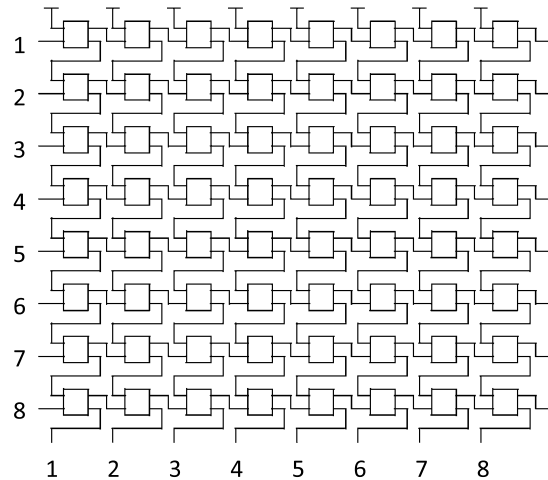
continuously with an analogue driving signal. Larger digital switches can be implemented with multiple 2×2 (or 1×2) switches. Figure 10.2 shows an $N \times N$ crossbar switch architecture that uses 2×2 switches as basic switching elements, arranged in N horizontal lines and N vertical lines in a 2D plane. Each cross point has a switching element and in total N^2 switching elements are needed. A crossbar switch has intrinsic non-uniform insertion loss due to different path lengths and different numbers of switching elements for different connections.

The 2×2 switches of an $N \times N$ crossbar architecture can also be arranged in such a way that light from any input to any output port passes N switching elements resulting in path-independent insertion loss (PI-IL) [7, 8]. Both, the general and the PI-IL crossbar switch architectures are strictly non-blocking. There are other architectures that use smaller numbers of switching elements, e.g. the Benes architecture [9] but depending on the structure of such switches these architectures may cause switches to be blocking. Larger switching matrices using digital actuators do generally suffer from higher insertion loss since IL increases proportionally to the amount of switching elements in the light path. In addition, crosstalk from each 2×2 switch accumulates in the case of multistage switches, which is another drawback.

Optical Switch Architectures Using Analogue Actuators Analogue actuators, including MEMS mirrors, liquid crystal devices, and piezo-electric actuators, can move an optical beam freely to multiple space positions so that a single actuator enables a $1 \times N$ optical switch.

With $2N$ $1 \times N$ optical switches arranged in an architecture proposed by Spanke a strictly non-blocking $N \times N$ switch can be achieved [10]: Each input port directs the incoming beam to the appropriate output $N \times 1$ switch which then switches the signal to the output port. Corresponding switches become complicated for large port numbers N since there are N^2 optical fibers to be physically interconnected. However, the design can be made better scalable if the interconnects are realized as free space $1 \times N$ and $N \times 1$ switches at the input and output, respectively, resulting in $2N$ actuating elements for an $N \times N$ switch with analogue actuators.

Since 2D analogue actuators can steer optical beams along two axes so that the optical beams are traveling in 3-dimensional space inside the switch, switches of this

Fig. 10.3 Required switching element number vs. switch port count for 3D switch architecture with analogue actuators, Benes network, and 2D crossbar switch
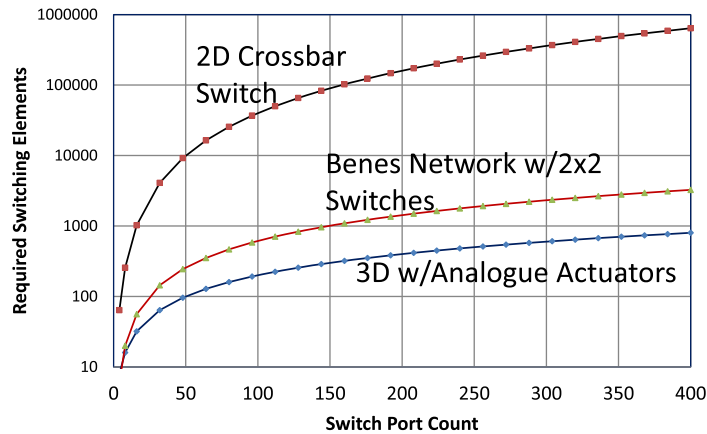
kind are typically called 3D optical switches. On the other hand, integrated crossbar switches using digital actuating elements are called 2D optical switches.

The number of required switching elements scales differently as the number of ports gets larger as illustrated in Fig. 10.3 for (i) 2D crossbar, (ii) Benes switches based upon 2×2 switches, and (iii) 3D analogue $N \times N$ switches, and the advantages of analogue actuators for larger $N \times N$ switching fabrics is obvious.

Clos architecture for Very Large Scale Optical Switches   Clos proposed a scheme to build large scale non-blocking $N \times N$ switches by using multiple smaller switches in three stages and requiring fewer crosspoints than a complete crossbar [11]. Key features are: a first stage with $m = \frac{N}{n}$ non-blocking $n \times k$ switches (n inputs, k outputs), a second stage consisting of k crossbar switches of size of $m \times m$, and a third stage consisting of m non-blocking $k \times n$ switches with k inputs and n outputs.

A Clos network is a strict-sense non-blocking switch if $k \geq 2n - 1$, and it is re-arrangeably non-blocking if $k \geq n$. In addition, it can also be implemented in a folded architecture [12].

10.1.4 Wavelength Selective Switches (WSS)

10.1.4.1 General Aspects

A wavelength selective switch (WSS) [13–17] is a device capable to switch optical wavelengths between several optical fibers. Each fiber carries multiple DWDM wavelengths, and wavelength selective means selectively switching a particular wavelength between fibers. WSSs are blocking in the wavelength domain since there is no wavelength conversion inside the switch.

Being hitless is a feature required for most telecom systems [15]. Although the telecom system can use non-hitless WSSs to implement hitless operation, it is desirable for WSSs itself to be hitless. For a WSS that is non-hitless, the switched

wavelength may be swiping through (the) other un-intended channels shortly during the transient time of switching. For a hitless WSS, this does not happen. That means when switching a wavelength with the hitless WSS, only the specific wavelength in the present port and the target port are affected, while all the other wavelengths and other ports won't be affected.

Currently (most) optical transmission systems align operation wavelengths to the traditional ITU standard with 50 GHz and 100 GHz channel spacing. However, tighter channel spacing (25 GHz, 33 GHz) or 87.5 GHz instead of 100 GHz might enable higher total transmission rates per fiber [16], and in order to be compatible with such systems, flexible grid or gridless operation of WSSs has been proposed as a future proof technology. To enable gridless operation of a WSS, 12.5 GHz or 25 GHz granularity is required, and as a consequence much more actuators ($4\times$ for 12.5 GHz or $2\times$ for 25 GHz granularity) are needed for a WSS with 50 GHz channel spacing. Technologies like liquid crystal on silicon (LCoS) have no problem in offering more pixels but for others like MEMS it is difficult to do so. Currently, most WSSs are specified for operation at fixed ITU grid frequencies with either 50 GHz or 100 GHz channel separation. However, how important future proof flexible grid WSSs might be, is a matter of ongoing and controversial discussion.

10.1.4.2 Optical Architectures for 1 × N WSSs

A $1 \times N$ WSS can be constructed with discrete components such as demultiplexers (demuxes), switches, and multiplexers (muxes), but such a switch will be bulky with hundreds of fiber terminations to interconnects. This is unfavorable for telecom applications, where device size, i.e. small WSS footprint, has become particularly important. Furthermore, cascading discrete demux/mux components narrows the device wavelength passband, which makes this approach even less attractive.

Currently most $1 \times N$ WSSs deployed in reconfigurable optical add-drop multiplexers (ROADMs) use diffraction grating-based free-space-optics coupled with an optical switching engine [16, 17]. The switching engine manipulates the particular wavelengths from one port to another by changing the phase, polarization, angle or position of a wavelength-dispersed optical beam. The switching engine can use digital or analogue actuation elements as described in Sect. 10.1.3.2.

The diffraction grating in a WSS is usually in the Bragg or Littrow configuration, where the diffraction angle of the -1st order is equal to the incidence angle for the central wavelength [18], see also Chap. 9, Sect. 9.5. The diffraction grating for WSSs is designed to have maximum diffraction efficiency (e.g., $>90\%$) in the Bragg configuration.

In recent WSS designs, the ports are typically arranged as 1D arrays of fibers or fiber collimators at the input/output as shown in Fig. 10.4(a). These linear ports are arranged parallel to each other, and different wavelengths, after passing the optical lens, will be focused to different positions in the back plane of the optical lens where the optical switching elements are located. These switching elements redirect each individual input beam to the selected output port.
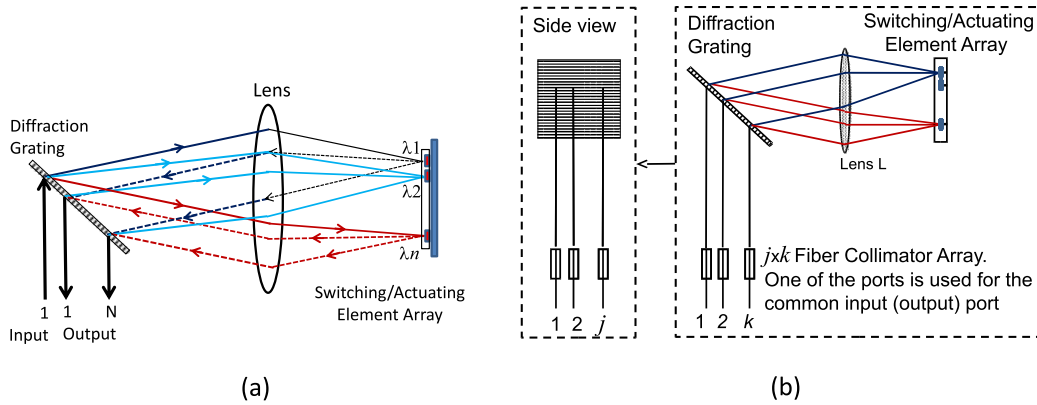
Fig. 10.4 $1 \times N$ WSS basic architecture. (**a**) Input/output ports in a 1D array, (**b**) input/output ports in a $j \times k$ 2D array

The direction of the port spreading may be either parallel or perpendicular to the direction of wavelength spreading produced by the grating (as shown in Fig. 10.4(a)). If it is parallel, then adding more ports increases the size of the optics in the wavelength dispersion direction and the optical design needs to consider the different path lengths. If it is perpendicular, which is more common in current WSS designs, then adding more ports increases the size of the optics perpendicular to the dispersion direction.

The switching elements can steer the beam in two axes, therefore it is possible to arrange the input/output fibers in 2 dimensions as $j \times k$, so that it is possible to increase the device size along two axes. Figure 10.4(b) shows the schematic of a $1 \times N$ WSS switch with an $j \times k$ 2D configuration for the input/output ports.

Switching/actuation of $1 \times N$ WSSs may be achieved by 1D arrays of MEMS mirrors, polarization-based liquid crystal arrays, or LCoS-based phase only spatial light modulators (SLM), or other types of actuating devices.

For 1×2, 2×2 and some of the $1 \times N$ WSSs, digital switching elements like polarization liquid crystal cells or Texas Instruments digital micromirror devices (TI DMD), i.e. digital MEMS mirrors, can be used [19]. However, most of the $1 \times N$ switches use analogue switching elements such as 3D MEMS mirror arrays or LCoS phase only SLMs for optical beam steering.

10.1.4.3 $M \times N$ WSSs

An $M \times N$ WSS is also called a wavelength selective cross-connect (WSXC) [13, 14]. The designation $1 \times N$ or $M \times N$ refers to the fiber terminals and is essentially equivalent to the switch matrix size. A WSS can handle m DWDM wavelengths, e.g., $m = 40$ or 96. These channels are separated by 50 GHz or 100 GHz according to the ITU grid. A 50 GHz channel spacing, n channel $M \times N$ WSS means (a) The WSS under consideration has M input fiber terminals and N output fiber terminals, (b) each WSS terminal fiber carries n DWDM wavelengths, (c) the WSS has n $M \times N$ switches, one switch for each wavelength, and (d) the DWDM wavelengths have a channel spacing of 50 GHz.

Fig. 10.5 $M \times N$ wavelength selective cross-connect with n wavelength
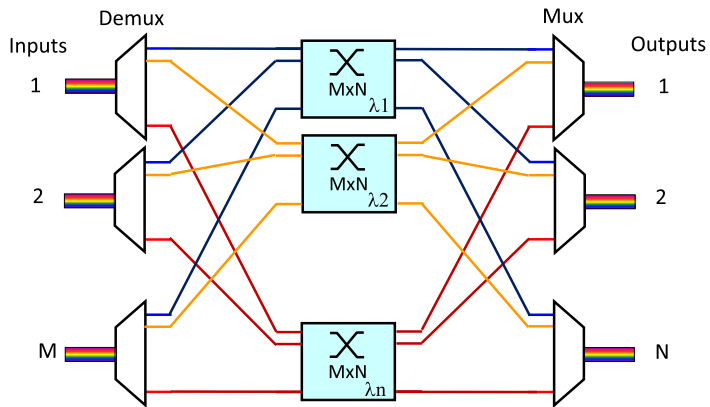
In principle, $M \times N$ WSSs can be built with the same grating technologies as $1 \times N$ WSSs to separate wavelengths in space while a 3D $M \times N$ switch architecture is used for space switching. It is highly desirable to build $M \times N$ integrated wavelength selective switches due to their low cost and low loss nature. The schematic of an $M \times N$ WSS capable of handling n wavelengths is shown in Fig. 10.5 [13–15], and a specific $M \times N$ optical wavelength selective (n wavelengths) optical cross-connect switch architecture as proposed by Solgaard [20] is illustrated in Fig. 10.6. This $M \times N$ switch uses 2D arrays of switching/actuating elements to implement

Fig. 10.6 $M \times N$ WSS. (**a**) Diffraction grating separating the wavelengths from multiple inputs into an $N \times n$ parallel beams. (**b**) $N \times N$ WSS architecture using two switching element arrays
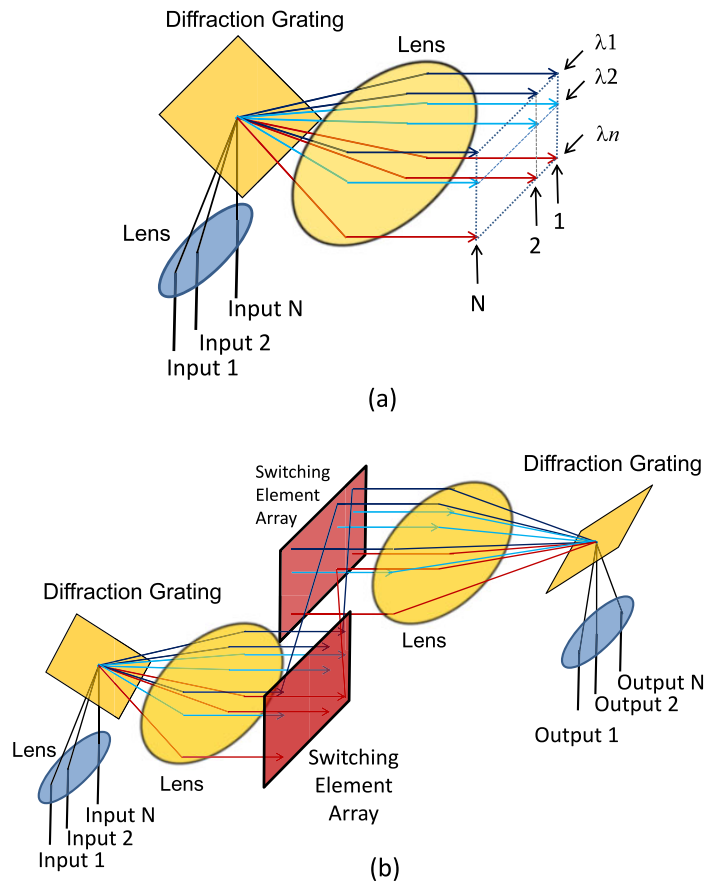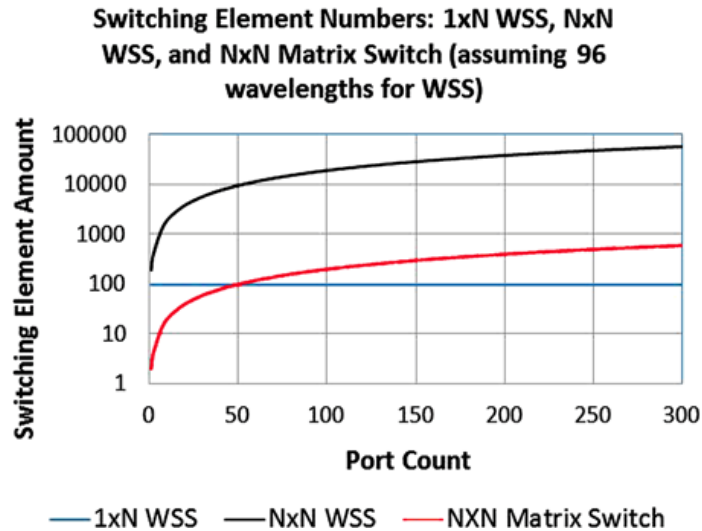
Fig. 10.7 Comparison of
minimum switching elements
needed to build $1 \times N$ WSS,
$N \times N$ WSS, and $N \times N$
matrix switch (assuming
$1 \times N$ and $N \times N$ WSSs to
have 96 wavelength channels)

the full-functionality of $M \times N$ ports optical wavelength switching. Each connection
(i, j, λ_k) needs two switching elements to steer an input beam to the output mirror
and steer the output mirror to let the beam to point to the right output port. A diffraction grating separates the multi-wavelength signal into individual wavelength channels (Fig. 10.6) in such a way that different wavelengths are all spread in one direction, and light from different input fibers is spread perpendicularly to the wavelength
spread direction. After the lens, wavelengths from one input fiber are separated vertically, and the same wavelengths from different input fibers are lined up horizontally.

Input and output fibers are arranged to have parallel demultiplexed beams (see
Fig. 10.6(a)), and these are coupled with a matrix switching system using two
switching element arrays (see Fig. 10.6(b)) so that a fully functional $M \times N$ WSS
is obtained. The switching/actuation elements need to be analogue, and the total
amount of required switching elements is $(M + N) \times n$. The switching elements can
be 3D MEMS or LCoS. A comparison of the minimum number of switching elements needed for $1 \times N$ WSS, $N \times N$ WSSs and $N \times N$ matrix switches as shown
in Fig. 10.7 demonstrates the difficulties in designing $N \times N$ WSSs because the
number of required switching elements increases very rapidly with port count. Today's largest commercially available optical matrix switch port count is 320×320,
which has about 640 switching elements [21], and for a 96 wavelength 4×4 WSS
a total of 768 switching elements is required.

10.1.4.4 Multicast Optical Switches

An $M \times N$ multicast switch is a unidirectional switch that can route any input port
to any one or to multiple (up to N) output ports [22, 23]. The operation principle is
(i) splitting any incoming light at each input into N optical beams, (ii) connecting
each split portion to a different $M \times 1$ switch, and (iii) setting each switch in such
a way that the channel(s) wanted pass to the corresponding output. The output port
count determines the splitting ratio, the typical number of output ports of this switch

varies from 4 to 24, and if the output port number is large, the IL is correspondingly high due to the high splitting ratio. This architecture is called Broadcast and Select, which we call multicast switch type "A".

Another type of multicast switch ("type B") uses a larger optical switch for optical switching and the splitting ratio can be customized to different ratios. For example, if we use $1 \times L$ splitters for the input ports, the multicast switch can only route at most L ($L < N$) ports to any L output ports, and in order to make type B multicast switches strictly non-blocking, an $(M \cdot L) \times N$ matrix switch is required.

Most currently available multicast switches are of type A and are based on PLC technologies. Switch sizes include 2×8, 4×4, 4×8, 8×8, 8×16, and 8×24 [23]. Type B multicast switches offer better flexibility in fiber interconnects but need large-scale optical matrix switches.

10.2 Opto-Mechanical Switches

Small opto-mechanical 1×1, 1×2, 2×2 and $1 \times N$ switches have been widely used in telecom systems in central offices and in un-controlled environments. These optical switches have been among the first commercially available ones and have been widely deployed for protection and restoration and are widely used for optical testing for about 40 years [24].

The switching function of opto-mechanical switches relies on mechanical actuation [24], accomplished by mechanically moving or rotating fibers, prisms, or mirrors. Opto-mechanical switch design involves collimated optics, free space optics and fiber coupling, and specially designed optical components in a mechanical moving mechanism.

10.2.1 Fiber Collimators

Fiber collimators are used to either couple light from free space into an optical fiber or collimating light from a fiber to form a "collimated" optical beam. The basic structure of a fiber collimator consists (in most cases) of at least a lens and an optical fiber. Lenses which can be used include fiber lenses, ball lenses, aspherical lenses, spherical singlets and doublets, GRIN (GRaded INdex) lenses, microscope objectives, or cylindrical lenses. In the case of thermally expanded core (TEC) fiber no lens is needed at all. Lens materials vary from glass to silicon. Currently, most fiber collimators use GRIN lenses [25, 26] or so called C-lenses [27]. A C-lens is a miniature lens with similar performance as a GRIN lens but slightly better insertion loss, lower cost, and longer working distance compared to GRIN-lens collimators, so that C-lens fiber collimators are more popular for micro-optic devices.

Furthermore, collimators can be single fiber or multiple fiber collimators using a single lens or multiple fibers with multiple lenses to form a fiber collimator array. Their diameters can be as small as the fiber itself, for example 125 μm, or as

large as tens or hundreds of millimeters, all depending on the optical design and purpose. Based on optical beam waist size and waist position the optimum working distance can be determined. Another important specification for fiber collimators is insertion loss, which is due to the lens and coupling imperfections. The alignment tolerance for insertion loss due to misalignment and beam spot size mismatch of two collimated Gaussian beams was treated in [28–30].

10.2.2 Opto-Mechanical Actuators

An opto-mechanical actuator controls or moves optical parts, and opto-mechanical switches require actuators. These may typically involve a relay, a solenoid, a drive motor, a deflection opto-mechanical scanner, or other mechanical rotation components or even a high precision mechanical robotic arm for larger switches [32–44]. The actuators under consideration here produce either linear (straight line), rotary (circular), or oscillatory motion and are typically driven with electric current. One important feature of an actuator is to have a latching mechanism which ensures that, after the end of the movement, the switch will remain in its actual status/position and does not need any additional power to hold the moveable part in position.

The opto-mechanical actuators most widely used for optical switches are solenoid relays and stepper motors, and their most important characteristics are accuracy, speed, and cost. Stepper motors can be used as a rotatory actuator which can move around a rotational axis to multiple positions (degrees), but the rotation of stepper motors can also be translated into a linear movement.

10.2.3 1 × 1, 1 × 2, 2 × 2 and Small Port Count N × N Opto-Mechanical Switches

1×1 (on/off), 1×2 and 2×2 opto-mechanical switches were the first optical switches available and have been widely used for over 30 years. These 1×1, 1×2, and 2×2 opto-mechanical switches have about 1 dB insertion loss, very high isolation, low crosstalk, and a switching time between 5 ms to 20 ms. They use a digital actuator, such as a solenoid-based electro-mechanical relay. 1×1 on/off switches only require a light blocker to be moved in and out of the light path, and 1×2 or 2×2 switches most frequently use solenoid electro-mechanical relays as digital actuators.

A simple 2×2 opto-mechanical relay switch may use two dual fiber collimators with a glass ferrule with 250 or 127 μm separation, a common collimating lens, and a reflective mirror on a relay as actuator [32]. When the reflective mirror is moved into the light path by the solenoid electro-mechanical relay, the switch is changed from the bar to the cross state. The structure is robust and has good misalignment tolerance due to the very short free space path length. Another widely used variety of 1×2 and 2×2 switches uses prisms (see Fig. 10.1 and [33–35]). Moving the prism

into the light path changes the switch from the bar to the cross state due to refraction of the prism. The prism can be moved vertically or horizontally, and the architecture can also be used for 1×1 and 1×2 switches. The cube prism architecture is very robust, and an angular misalignment of the prism will only generate a small lateral beam offset. Another variant of a 1×2 prism switch uses a prism with specific shape and takes advantages of dual fiber collimators with shared collimating lens, so that the cost for alignment, assembly, and materials is lower and the light path is more robust [35].

For achieving larger than 2×2 switches with opto-mechanical actuators, several approaches using electro-mechanically driven prisms to deflect optical beams in free space have been proposed, and 4×4 and 8×8 switches have been demonstrated [36, 37].

10.2.4 $1 \times N$ Opto-Mechanical Switches

$1 \times N$ opto-mechanical switches with larger N are available from many vendors and have been widely deployed for protection, restoration, testing & measurement, and monitoring in telecom applications. Compared to other kinds of optical switches, a $1 \times N$ switch is particularly simple since the switch can be implemented with a single analogue controlling opto-mechanical actuator.

A straightforward way to build a $1 \times N$ opto-mechanical switch is using a linear actuator for fiber movement, either along one axis or along two axes. The basic principle is shown in Fig. 10.8 with the input fiber loaded in a movable stage. Index matching glue or gel between the interface of input and output fibers reduces back-reflections.

Since the moving parts are optical fibers, the accuracy requirements for this actuator type are as high <0.5 μm in the linear moving direction and <0.5 μm fiber position accuracy, which can be achieved by using V-grooves on silicon, Pyrex glass, or fused silica substrates [31]. Instead of using fiber to fiber direct coupling, similar $1 \times N$ switches can be built using fiber collimator arrays instead of fiber arrays, however, this adds cost and also increases insertion loss. On the other hand, a collimated beam greatly reduces the insertion loss sensitivity for the switch since the beam spot size for a fiber collimator is typically 100 μm (depending on design), compared to a single mode fiber core of about 10 μm.

Although $1 \times N$ switches based upon moving fibers or collimators are simple, they exhibit several shortcomings: (a) the displacements required are large, which

Fig. 10.8 Basic architecture of a $1 \times N$ optical switch that moves the input fibers using a stepper motor linear actuator
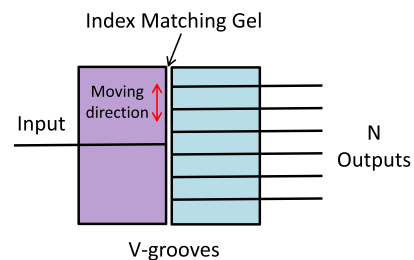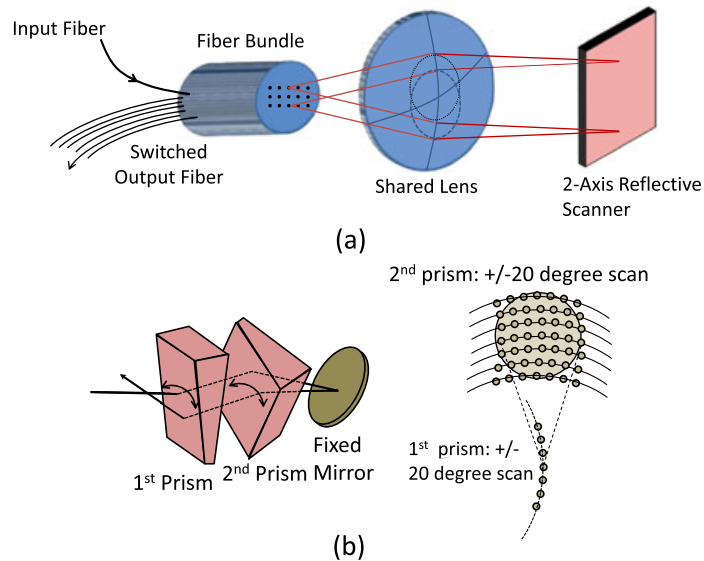
Fig. 10.9 Basic architecture
of an $1 \times N$ optical fiber
bundle switch by using a
2-axis reflective scanner
[38, 39]. (**a**) Fiber bundle
scanning switch architecture,
(**b**) high-resolution scanner
that enables beam deflection
by two rotating prisms

ultimately limits the switch size, (b) switching time may not be uniform and depend on fiber position (c) moving fibers or fiber collimators may cause dynamic crosstalk. This might require special measures in order make switching to be hitless.

Ford and DiGiovanni have proposed a fiber bundle scanning switch, illustrated in Fig. 10.9(a), which offers a cost effective approach for large $1 \times N$ switches [38, 39]. The input and all output fibers are carried in one fiber bundle and share a single lens. A two axis moveable reflective scanner in the aperture stop back-reflects incoming light with an appropriate deflection angle so that it can be coupled into any output fiber. The cost of a fiber bundle switch is nearly independent of the number of outputs, in contrast to switches with individually lensed fibers, and the number of outputs is only limited by the scan area and the density of fibers held in the bundle.

Figure 10.9(b) shows a high-resolution scanner that enables beam deflection by two rotating prisms held between a lens and a fixed mirror. When one prism is rotated, the spot on the bundle is deflected along an arc whose radius is set by the prism wedge and the lens' focal length. By rotating both prisms, the spot can be positioned anywhere within a 2D area. The smaller the prism wedge angle, the smaller the arc swept out by the prism rotation so that the full angular excursion of a mechanical rotational actuator can be mapped into an arbitrarily small scan angle. With appropriate lens focal length and prism deflection, the full mechanical scan range matches the active area of the fiber bundle. Corresponding switches can have hundreds or even thousands of ports, e.g. 1×160 has been demonstrated and 1×4096 has been designed [38, 39].

10.2.5 *Large Scale N × N Opto-Mechanical Switches with Robotic Arms*

Robotic optical switches with large scale $N \times N$ non-blocking cross-connect functionality have been developed for quite some time [40–48]. Although there are ap-

Fig. 10.10 Schematic of $N \times N$ optical switch based on robotic motor arms, arms can move in/out fibers in x-direction and y-direction, respectively [45, 46]
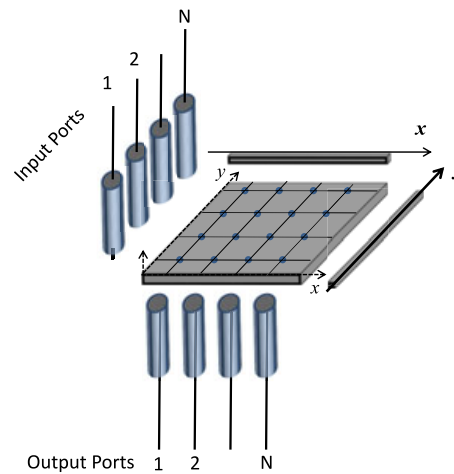
proaches of using fiber collimators for non-contact robotic optical switching, typically the large scale $N \times N$ robotic switches physically connect two optical fibers together without mirrors, lenses, or collimators, in exactly the same way that fiber connectors mate. Instead of doing so manually, the mating is done by robotic motor driven arms.

The robotic $N \times N$ approach was first described by Sjolinder with opposing fiber connectors translating independently along separate, orthogonal, linear tracks in two separate parallel planes so that any input optical fiber and any output fiber can be coaxially aligned at an array of insertion points formed between the two planes, as shown in Fig. 10.10 [45]. Based on this concept, FiberZone developed a robotic optical switch based on a three-layer architecture with two active layers in which robotic motors position input (or source) and output (destination) fibers in an x- and y-plane, respectively, and a passive connection layer or adaptor layer where connections are latched in place [46]. After completing a latched connection, the switch systems are functionally equivalent to a manual patch panel with its purity of signal and low loss characteristics. Transmission of optical signals maintains full connection integrity, even if electrical power is lost.

Since each input and each output fiber is moved in a straight line, fiber entangling is no issue. However, because all input (output) fibers need to be arranged in a row (column), raising the switch size to more than 200×200 ports is difficult but 180×180 port switches are commercially available [47].

Kewitsch proposed another way to build large scale $N \times N$ switches using a robotic motor actuator offering 1000×1000 switching capacity. This architecture uses a single robotic motor actuator to do 3-axis pick-and-placement [48].

Based on this architecture, Telescent [49] developed an all-fiber, robotically reconfigured cross-connect that is scalable up to a true non-blocking 1008×1008 switch, based upon 48 modules enabling a pay as you grow strategy. The insertion loss is identical to that of a manual patch panel by utilizing standard LC/PC, LC/UPC, or LC/APC connectors. This flexible patch-panel is a latching matrix switch.

The drawbacks of this flexible robotic $N \times N$ switch include: (a) switching time is slow, typically 1 minute per connection, (b) switching cannot be done in paral-

lel but in the 1 minute time frame one connection can be made only (c) it may be difficult to reduce cost since each port needs individual assembly (e) repeatability depends on cleanliness of connectors (which have to be cleaned), (f) mating durability is limited, connectors can be plugged in about 1000 times, after that reliability may degrade.

10.3 Liquid Crystal (LC)-Based Optical Switching

10.3.1 Operating Principals of Liquid Crystal Material for Optical Switches

Liquid crystals (LC) are rod-like molecules in a state of matter that goes from crystalline $\rightarrow$ smectic $\rightarrow$ nematic $\rightarrow$ liquid as it is heated [50]. The optical properties (refractive index and birefringence) of LCs depend on molecular orientation [51, 52] and can be controlled by applying relative modest electric fields across LC cells, and the change of the optical properties can be exploited to build 1×2, 2×2, and larger $N \times N$ optical switches, and in particular, $1 \times N$ wavelength selective switches [52–54].

Liquid crystals are used in two ways for optical switching: (i) as programmable polarization rotator and acting as digital actuator [55], or (ii) as programmable spatial phase modulator for performing spatial beam steering and acting as analogue actuation element [56]. Both, operation in transmission or reflective configurations are possible. Depending on the alignment of the LC molecules (typically either parallel, vertical, or twisted), phase only, amplitude, or polarization of an incident light beam are modified. Currently the most frequently used liquid crystal types are parallel aligned nematic (PAN), twisted nematic (TN), and smectic liquid crystals.

Liquid Crystal Polarization Switching Principle Both parallel aligned nematic and twisted nematic liquid crystal cells can be used as a controllable polarization rotator. Without applied voltage such cells continuously rotate incoming linearly polarized by 90°, i.e., s-polarized light is rotated to p-polarized light while p-polarized light is rotated to s-polarization, as shown in Fig. 10.11(a) and (b). On the other hand, when an appropriate voltage is applied to the LC cell, it behaves like a piece of glass and both, s- and p-polarized light, keep their original polarization (Fig. 10.11(c) and (d)).

For polarization induced switching a half-wave retardance is required as a half-wave retarder can rotate the polarization of linearly polarized light to twice the angle between the retarder fast axis and the plane of polarization. Therefore, placing the fast axis of a half-wave retarder at 45° to the polarization plane results in a polarization rotation of 90°.

For switching the polarization state between two angles only, for example 0 and 90°, a twisted-nematic device is an excellent solution as it has a very simple driving scheme [55, 57]: a high voltage (e.g. above $\sim$5 V) gives 0 rotation and a low voltage

Fig. 10.11 Functionality of
LC polarization rotator
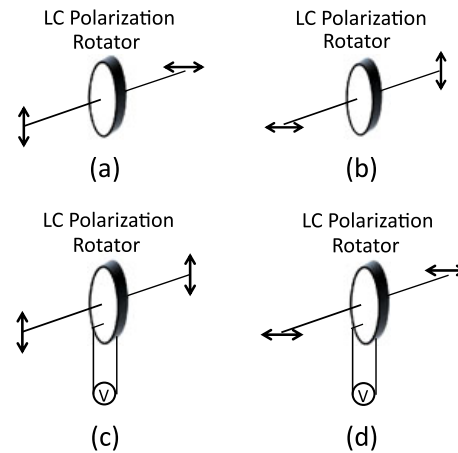
(e.g. below ∼0.5 V) gives 90° rotation, so that no tight control of operation voltage is required nor are temperature changes an issue.

Multiple elements of TN or PAN LC polarization switches can be easily fabricated by appropriately patterning an indium tin oxide (ITO) film on top of the LC. ITO is transparent and electrically conducting and can be deposited as a thin film. With a specially patterned ITO layer containing multiple electrodes, the pixels can be controlled and switched (on/off) individually with an electric field.

Liquid Crystal Spatial Light Modulator Operating Principle   A liquid crystal spatial light modulator (LC SLM) has a pixel array of LC cells [56]. Both PAN and TN LCs can be used for SLMs, and LC SLMs can be either transmissive or reflective. An example of an LC SLM is a transmission PAN liquid crystal display (LCD) SLM.

LCD SLMs based on transmissive LCD technology frequently have a small pixel fill factor (around 60%), and the relatively large amount of optically inactive space makes it difficult to achieve hitless and flexible passband operation. In addition, compared to reflective solutions, the thickness of the LC layer needs to be doubled.

Another important LC SLM technology is liquid crystal on silicon (LCoS) [58, 59]. LCoS technology has been developed for many years for image and video display applications. This technology combines the unique light-modulating properties of LC materials and the advantages of high-performance silicon complementary metal oxide semiconductor (CMOS) technology through dedicated LCoS assembly processes. An LCoS device is reflective. LCoS SLMs can be used to modulate the amplitude, phase, and/or polarization of optical beams with different configurations and LC alignments. The architecture of LCOS devices is similar to that of conventional LC devices except that a silicon backplane constitutes one of the substrates.

A schematic of an LCoS structure is shown in Fig. 10.12.

The silicon CMOS backplane comprises high-performance driving electronic circuitry, buried underneath the pixel array(s), which has (have) a very high fill factor (>99%). The pixels are aluminum mirrors deposited on the surface of the silicon backplane, typical sizes are in the range of 3 to 32 μm, and chips with XGA resolution have 1024 × 768 pixels, each with an independently addressable voltage so that
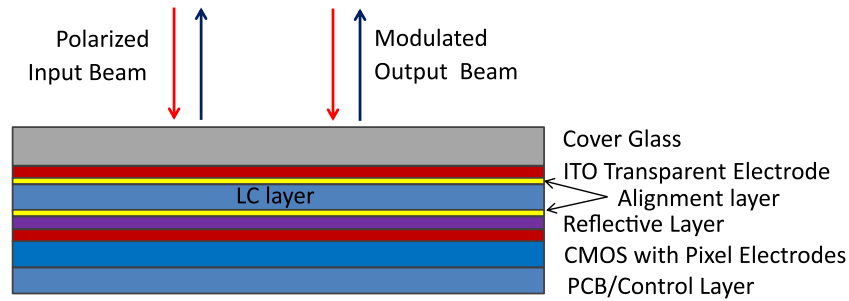
Fig. 10.12 Liquid crystal on silicon spatial light modulator basic structure [58, 59]

the phase retardation of each pixel can be controlled. Typical LCoS cell dimensions are: 1 to 3 cm² size, ~2 mm thickness, and a minimum pixel pitch of ~2.8 μm. A common voltage for all pixels is supplied by an ITO layer on the cover glass. The dimensions of the LCoS cell are determined by the pixel size and the pixel pitch.

For optical switching LCoSs are typically operated as spatial phase modulators, and both PAN and TN LC technology can be used for "phase only" LCoS SLMs. If the polarization of the incident light beam is parallel to the slow optical axis of a PAN LCoS device, and if an appropriate phase distribution has been generated across the pixels of the SLM, optical beam steering is achieved [60, 61]. For appropriate beam steering the phase modulation required is at least 2π in order to fully modulate the phase of each pixel.

The principle of optical beam steering using LCoS SLMs is the same as phased array beam steering. The diffractive optical phased array can be thought of as a quantized, programmable multiple level phase grating [60]. As illustrated in Fig. 10.13 each ramp comprises several LCoS pixels, each pixel with an increasingly larger phase delay, ranging from zero to 2π.

Detailed descriptions of the general characteristics of diffraction gratings can be found in physics or optics text books (see also Chap. 9, Sect. 9.5) and will not be repeated here. For beam steering the first diffraction order is usually chosen since it has the highest diffraction efficiency.

Fig. 10.13 Generating a digitized liquid crystal phase grating using spatial light modulation
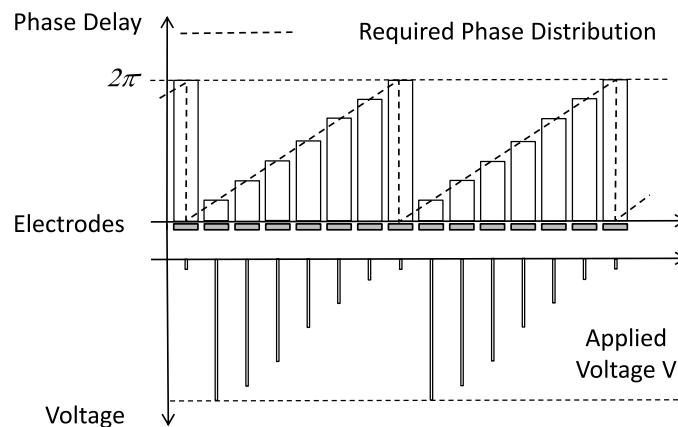
The more phase levels are used in the array, the closer the ramp comes to an ideal ramp (instead of stair steps), and the higher the diffraction efficiency [60]. For example, a binary phase grating ideally provides a diffraction efficiency of 40.5% in each of the two first order diffracted beams. For a quantized phase grating using three phase levels/pixels the ideal first order diffraction efficiency is 68.4%, and it increases to 81% (87.5%, 94.9%) for 4 (5, 8) phase levels/pixels, respectively.

LCoS-based beam steering results in highly wavelength dependent switches in contrast to fairly wideband operation of TN LC polarization switching. Therefore optical space switches typically use TN LC polarization switching if wide passbands are required. On the other hand, WSSs do not require wide passbands and therefore LCoS beam steering is typically used for WSSs.

10.3.2 Liquid Crystal Optical Matrix Switch: 1 × 2, 2 × 2, N × N and 1 × N Switches

1 × 2 Switches   The basic principle of LC polarization-based optical switches [57, 62–67] is illustrated in Fig. 10.14 where PBS and PS represent a polarization beam splitter and a polarization switch, respectively. It is obvious, that this 1 × 2 LC switch is polarization dependent.

Polarization independent optical switching even with polarization dependent LC devices can be accomplished, and Fig. 10.15 illustrates one example of turning the polarization dependent 1 × 2 switch shown in Fig. 10.14 into a polarization independent 1 × 2 switch using polarization diversity optics. The beam displacing prism (BDP) separates the un-polarized light into s- and p-polarized beams. The p-polarized beam passes the half-wave plate (HWP) and is changed to an s-polarized

Fig. 10.14 Liquid crystal polarization switch-based 1 × 2 polarization dependent optical switch. (**a**) Switch to output 1, (**b**) Switch to output 2. PBS: polarization beam splitter, LC: liquid crystal, PS: polarization switch
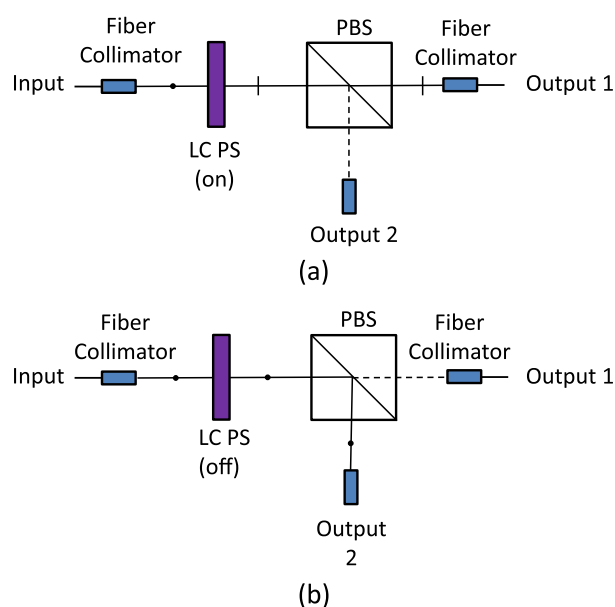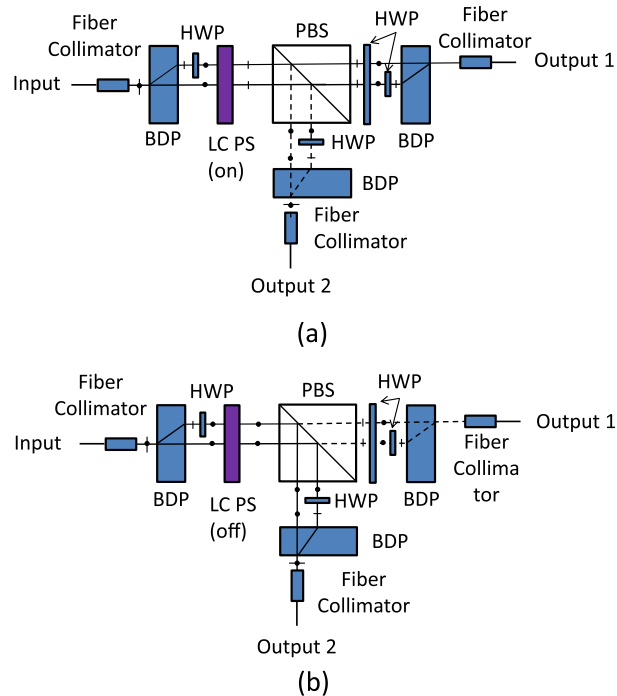
Fig. 10.15 Liquid crystal polarization switch-based 1 × 2 polarization independent optical switch using polarization diversity optics. (**a**) Switch to output port 1, (**b**) Switch to output port 2. BDP: beam displacing prism, HWP: half-wave plate, PBS: polarization beam splitter, LC: liquid crystal, PS: polarization switch


beam. When the PS is in its "on" state, both beams are switched to p-polarization and pass through the PBS and the HWP. After that both beams are changed to s-polarization, pass through the polarization combining optics and are coupled into output port 1 (Fig. 10.15(a)). When the LC PS is in its "off" state, both beams remain s-polarized, are reflected by the PBS, combined by the polarization combining optics and coupled into output port 2 (Fig. 10.15(b)).

LC polarization switching typically has a polarization extinction ratio of about 20 to 25 dB, which is generally insufficient to meet crosstalk requirements of optical switches. Double LC-PS elements in the light path enable to achieve double crosstalk rejection so that the crosstalk level can be improved significantly.

Figure 10.16 illustrates how first order crosstalk from the first LC-PS1 can be removed from the light path. When PS1 and PS2 are in the "on" state (Fig. 10.16(a)), the switch is in the 1 → 1 state. First order crosstalk from PS1 is s-polarized light. It is reflected by PBS to PS3 which is in its "on" state and changes the first order s-polarized light to p-polarization, and as a consequence it is directed to other spots instead of being coupled to output port 2. When PS1 and PS3 are in their "off" state (Fig. 10.16(b)), the switch is in the 1 → 2 state. First order crosstalk from PS1 is p-polarized light that passes through PBS to PS2, which is in its "off" state so that p-polarized light remains p-polarized and is directed out of the light path. By using this approach crosstalk of LC-PS-based optical switches can be improved to 40 to 50 dB.

In another configuration, but based upon the same principle, Fujii proposed to use PBS and BDP and four TN-LC devices to achieve low crosstalk 1 × 2 optical switching [65].

Fig. 10.16 Optical crosstalk reduction by using two LC-PS elements in a light path. (**a**) First order crosstalk removal in output port 2, (**b**) First order crosstalk removal in output port 1. HWP: half-wave plate, PBS: polarization beam splitter, BDP: beam displacing prism, LC: liquid crystal, PS: polarization switch

(a)

(b)
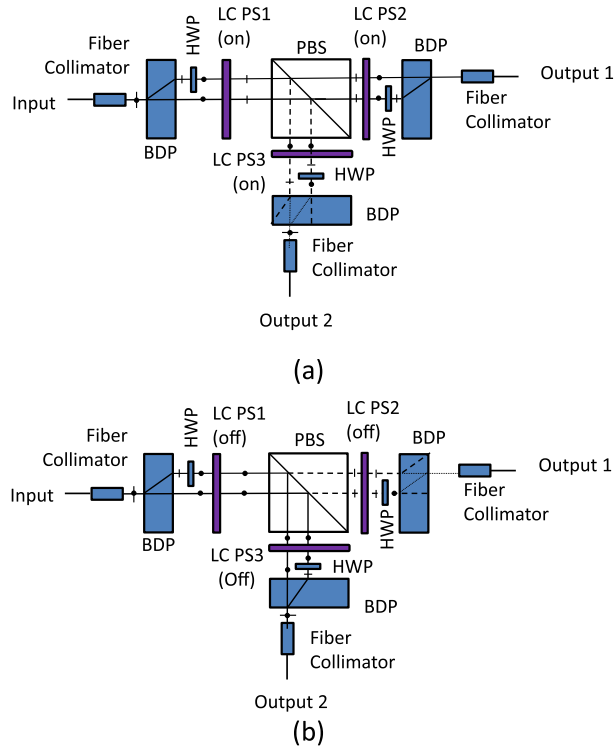
2 × 2 Polarization Independent Optical Switches LC-PS-based 2 × 2 optical switches with polarization diversity optics were reported by Wagner [62] and later by Soref [63, 64]. The 2 × 2 switch reported by Wagner used multi-mode fiber, but the switching architecture applies to single mode fiber switches as well. The schematic of the 2 × 2 optical switch, which uses a single LC-PS only, is shown in Fig. 10.17. When the LC-PS is in the "on" state (no voltage applied), the switch is in the bar state, i.e. $1 \rightarrow 1$ and $2 \rightarrow 2$ (Fig. 10.17(a)) while the "off" state (with voltage applied) to the LC-PS corresponds to the cross state of the switch, i.e. $1 \rightarrow 2$ and $2 \rightarrow 1$ (Fig. 10.17(b)). Since only one LC-PS cell is used, the crosstalk for this 2 × 2 switch structure is about 20 dB.

Polarization independent 2 × 2 switches with lower crosstalk, enabled by using four LC-PS elements, were reported in [66]. The concept is similar to that shown in Fig. 10.16 and ∼40 dB interchannel crosstalk has been achieved.

Liquid Crystal-Based 1 × N Optical Switches Both LC-PS and LCoS enable 1 × N optical switches. LC-PS-based 1 × N switches require multiple stages to enable multiple outputs. A total of $\log_2 N$ stages of LC-PS cascaded switching elements are required, and for the reduction of transient and static optical crosstalk another stage of LC-PS is needed to turn the target channel off before the actual signal is switched to that channel.

Figure 10.18 shows a 1 × 4 optical switch using three LC-PSs in two switching stages. The BDP1 and HWP are used for polarization diversity in the vertical direction. The BDP1 and HWP in the input side are used for separating the s- and p-polarized beams in the vertical direction (that is perpendicular to the paper sur-

Fig. 10.17 LC polarization switch-based 2 × 2 polarization independent optical switch using polarization diversity optics. (**a**) Bar state with LC-PS in off state, (**b**) cross state with LC-PS in on state. PBS: polarization beam splitter, TIR: total internal reflection prism

(a)

(b)
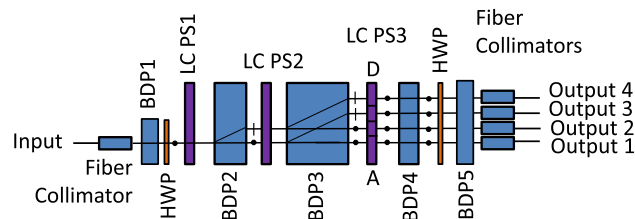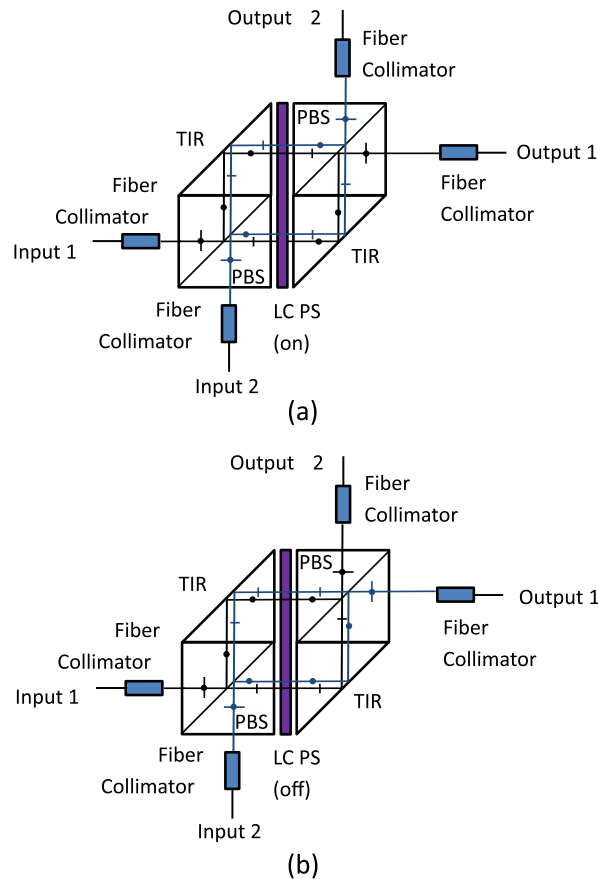
Fig. 10.18 Optical structure of the LC-PS-based 1 × 4 optical switch. LC PS: liquid crystal polarization switch; BDP: beam displacing prism; HWP: half-wave plate

face) and make both beams to have the same s-polarization direction. The HWP and BDP5 in front of the output ports are used for combining the two s-polarized beams in the vertical direction.

Recently, chiral smectic liquid crystals (SmC*) polarization insensitive binary phase gratings were reported. The LC is used as a programmable wave-plate and the advantage of this configuration is that it offers polarization insensitive binary phase modulators so that no polarization diversity is needed. Based on this, both $1 \times N$ and 8×8 switches were reported, however, with high IL [69–72].

Performance of Liquid Crystal-Based 1 × 2, 2 × 2, and 1 × N Switches   LC-PS-based 1×2, 2×2, and $1 \times N$ space switches have been developed and commer-

cialized in the past with reasonably good optical performance. These switches have typically less than 1.5 dB IL, about 45 dB optical crosstalk, 1 to 20 ms switching time, and they are very reliable with billions of switch cycles due to no moving parts. The switches operate over the whole 1.55 μm band but the passband is not as wide as that of opto-mechanical switches. In addition, LC-PS-based 1×2, 2×2, and $1 \times N$ optical switches require a large number of optical components and are more complicated than their opto-mechanical counterparts, which makes manufacturing more demanding. For this reason opto-mechanical or MEMS switches dominate the market for 1×2, 2×2, and $1 \times N$ optical switches.

Liquid Crystal-Based $N \times N$ Optical Switches   There were some proposals of building $N \times N$ space switches using LC-PS activation elements [68]. Basically, the 1×2 switching elements shown in Fig. 10.14 to Fig. 10.16 can be used to build $N \times N$ optical switches with crossbar architecture (see Fig. 10.2). However, these approaches are not very practical due to high loss and difficulties in manufacturing and packaging.

10.3.3 Wavelength Selective Switches Using Liquid Crystal Techniques

The first liquid crystal-based 1×2 and 2×2 WSSs were developed and manufactured by Corning Inc. [54]. 1×1, 2×2, and $1 \times N$ WSSs using LC PS devices have found widespread use [73] and are currently commercially available from CoAdna Technologies [74]. The other kind of widely deployed liquid crystal $1 \times N$ WSSs uses LCoS SLMs and has become commercially available first from Finisar [75, 79] and now from many vendors. Since liquid crystals easily scale in pixel number, these WSSs can handle 96 or more DWDM wavelength channels and are operational with flexible grid.

Liquid Crystal Polarization Switching-Based 1×2, 2×2, and $1 \times N$ WSSs
The switching core of $1 \times N$ WSSs are multiple $1 \times N$ switches. One implementation, proposed by Kelly and coworkers, uses LC-PS and birefringent wedges to direct the input optical beam to two or more output directions controlled by LC polarization switches [76], as illustrated in Fig. 10.19. The birefringent wedge deflects s-polarized light at a larger angle than p-polarized light, the polarization of the light hitting the wedge is controlled by the voltage across the LC PS cell, and as a consequence the output beam can be switched between two different output directions (Fig. 10.19(a) and (b)).

$1 \times N$ switches can be obtained by cascading $\log_2 N$ stages of such LC-PS and birefringent wedge assemblies as shown in Fig. 10.19(c). Finally, Fig. 10.19(d) shows a 1×4 switch based on two LC-PS/birefringent wedge assemblies plus a regular wedge prism to adjust the deflection angles of the beams to be symmetric. The four possible output beams exhibit two different polarization directions
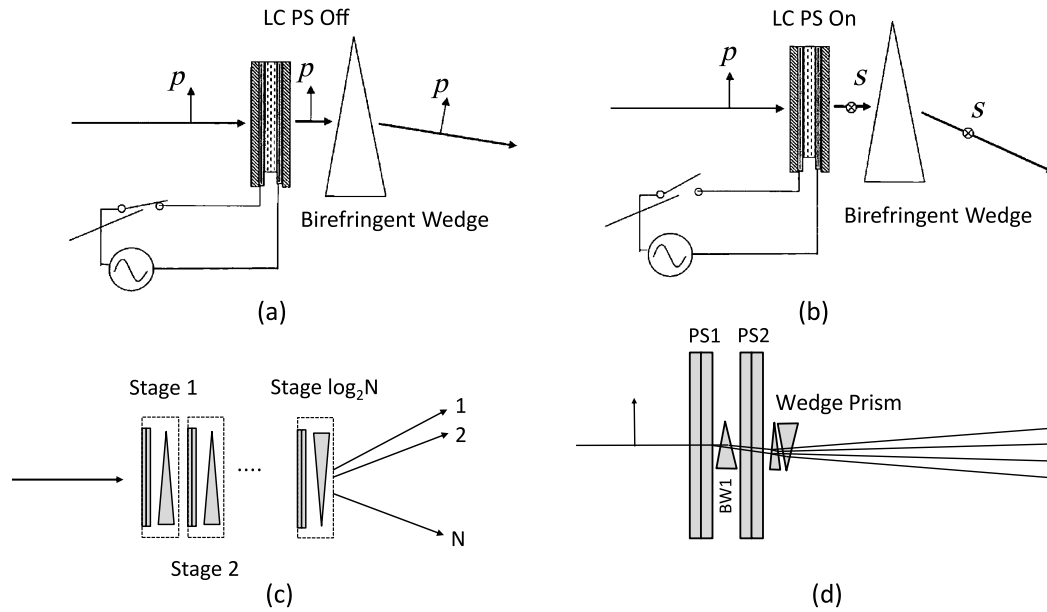
Fig. 10.19 Beam deflection by LC PS plus birefringent wedge(s) [76]. (**a**) Single LC PS stage in "off" state (voltage applied), (**b**) Single LC PS stage in "on" state (no voltage applied), (**c**) $1 \times N$ switch (schematic), (**d**) 1×4 LC PS switch with symmetric output
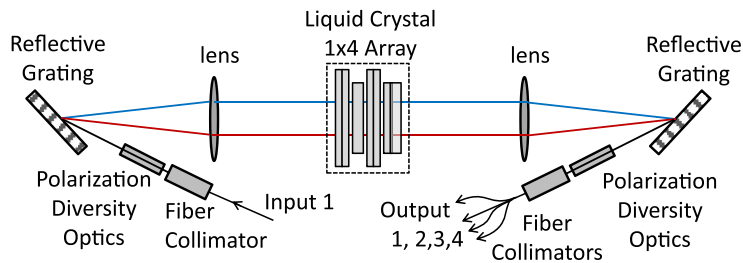
Fig. 10.20 Schematic illustration of 1×4 LC/wedge switching array-based WSS [76]

(Fig. 10.19(d)), and if that is not desirable, a third LC-PS may be added to manage the polarization directions so that all possible output beams have the same orientation of polarization.

Figure 10.20 shows an actual 1×4 LC/wedge switching array-based WSS. There are 1 input and 4 output fibers, and both input and output ports have fiber collimators and polarization diversity optics. A dispersive reflective grating separates the input beams into different angles according to the wavelengths.

The number of discrete wavelengths to be handled by a WSS determines the pixel number of the LC-PS array. A fixed (e.g. 50 GHz) channel spacing, 96 wavelength 1×4 WSS requires 96 pixels. For a flexible passband with 25 GHz resolution, the minimum number of pixels is 192.

LC-PS can operate either reflectively, transmissively or transflectively, but operating in reflective mode offers several advantages. A reflective device has a much smaller footprint and lower part count since a reflective device utilizes the same components for demultiplexing and multiplexing of the optical signals. In addition,

the optics of a reflective device is self-aligning in contrast to transmissive devices where the multiplexing optics must mirror the demultiplexing optics to a very high degree to obtain best performance. Also, double pass through the LC PS cell may improve the extinction ratio, the size of the channel blocking window, and switching speed.

There are many other kinds of $1 \times N$ WSS architectures using LC PS devices, however, the basic principle is still the same. Liquid crystal PS-based $1 \times N$ WSSs have been widely deployed for optical transport network and other applications. Commercially available $1 \times N$ WSSs have up to 30 output ports with variable attenuator function and packaged in a small package. Insertion loss is typically <5 dB with about 30 dB extinction ratio. These WSSs also offer flexible, flat top passband with 25 GHz resolution. Switching times are in the 1 ms to 100 ms range.

Liquid Crystal-on-Silicon-Based $1 \times N$ WSSs WSSs using LCoS switching elements rely on multiple phase gratings formed in LCoS technology where each phase grating is used for steering a particular wavelength to the output port wanted. The concept shown in Fig. 10.4 enables LCoS-based $1 \times N$ WSSs, however, due to various reasons these tend to be bulky and difficult to fit into a standard telecom shelf/blade and therefore alternative approaches are required.

Frisken proposed a modified LCoS-based $1 \times N$ WSS architecture that uses cylindrical lenses (CL) to handle the optics requirement of both the switching and wavelength axis [77]. Figure 10.21 shows a schematic of the $1 \times N$ WSS operating in reflective mode. The top view (Fig. 10.21(a)) shows the dispersion plane while the side view (Fig. 10.21(b)) shows the switching plane. The key points of this solution are: (i) CL1 and CL3 collimate light in the wavelength dispersion plane but do not affect light beams in the switching plane, while CL2 collimates light in the switching plane and does not affect light beams in the wavelength dispersion plane. (ii) The diffraction grating element (in transmissive mode) angularly separates the input wavelength channels into multiple channelized wavelength beams. (iii) The image of each of the spatially separated beams is a highly asymmetric ellipse ($\sim$700 μm $\times$ 25 μm) with its major axis in the switching plane, and the zones of the LCoS device match the elongated spatially separated wavelength bands.
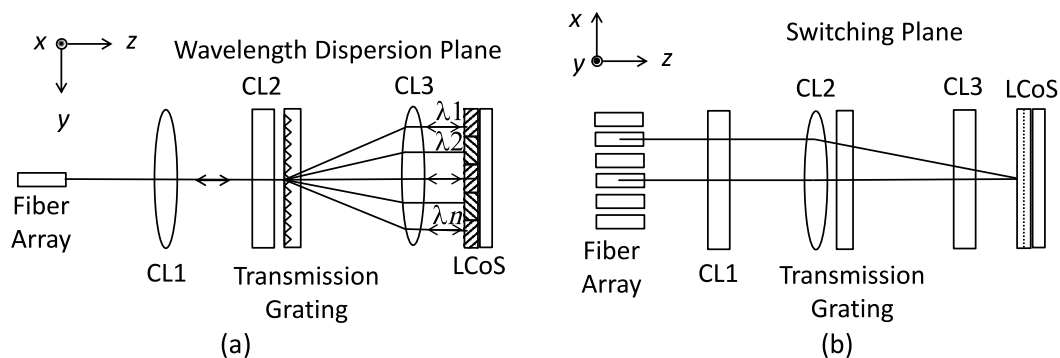

Fig. 10.21 Schematic representation of $1 \times N$ WSS operating in reflective mode (after [77]). (**a**) Top view illustrating wavelength dispersion plane, (**b**) side view illustrating switching plane. CL: cylindrical lens

Fig. 10.22 General concept of $1 \times N$ WSS using liquid crystal on silicon with polarization diversity optics, (**a**) perspective view, (**b**) top view [77]. FA: fiber array, MLA: micro-lens array, WP: Wollaston prism, BC: birefringent crystal, HWP: half-wave plate, CRM: cylindrical reflective mirror, RGP: reflective grating prism, RAP: right angle prism
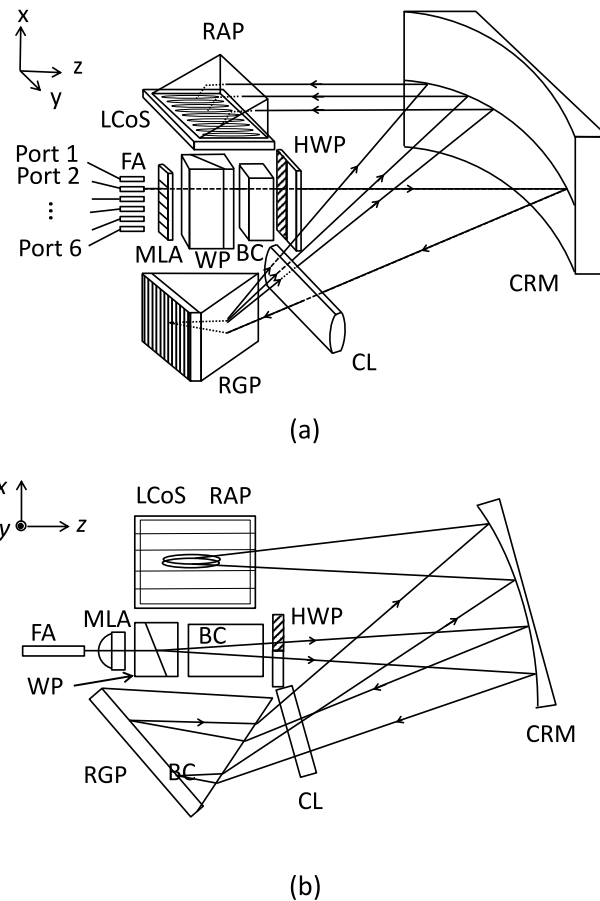
LCoS SLM switches have a number of advantages compared to MEMS solutions such as large modulation depths, no moving parts, low power dissipation, potential for large aperture operation, and low cost. Nematic LCoS devices are used for commercially available $1 \times N$ WSSs from Meadowlark Optics [55], HOLOEYE Photonics AG [59], Hamamatsu [80], and others.

A compact polarization independent $1 \times N$ WSS switch using an LCoS and a reflective grating is shown in Fig. 10.22 [77]. The design has been widely used for commercially available $1 \times N$ WSSs offered by Finisar Corporation [78, 79]. In this approach light is dispersed and focused in one plane and collimated in the orthogonal plane so that the LCoS utilized for switching between input and output ports operates on one polarization state of light only and this polarization diversity scheme does not require two sets of switching elements for the two polarization split beams (Fig. 10.22(b)).

Operation of the device can be understood from Fig. 10.22(a) where the various sub-components of the switch are: fiber array (FA), micro-lens array (MLA), Wollaston prism (WP), birefringent crystal (BC) e.g., YVO$_4$ or calcite, half-wave ($\lambda/2$) plate (HWP) assembly, cylindrical reflective mirror (CRM), reflective grating prism (RGP), and right angle prism (RAP). Any port can be chosen to be the input port and all others are the output ports. The BC and the HWP can be im-

plemented in such a way that polarization dependent path length differences are reduced, and furthermore the CRM can include a conic term in the definition of its curvature (to produce a cylindrical mirror) as an additional means for equalization path length differences of differently polarized beams, and as a consequence the WSS will have low polarization mode dispersion. The top view (Fig. 10.22(b)) illustrates the polarization diversity operation. If light from differently polarized beams overlaps in the same LCoS region, the same grating can be used for redirecting both images, and this is possible if light paths have been equalized sufficiently. The phase shift applied by the LCoS determines to which output port the light is directed.

There are applications that require a certain amount of coupling between ports including less efficient "images" for optical signal attenuation or optical power splitting, and these demands can be met by many different algorithms. There are also other ways to do polarization diversity, e.g. using two different LCoS zones for the two orthogonal polarization directions. That will double the control complexity, but requires less strict optics.

LCoS $1 \times N$ WSSs have become a mature technology that has proven itself in current applications of 50 GHz multiport WSSs for ROADMs. The introduction of flexible grid for $1 \times N$ WSSs doesn't introduce any new hardware requirements to be qualified and can be implemented on existing optical hardware designs without compromising in any way the reliability of the devices. LCoS-based $1 \times N$ WSSs can offer about 12.5 GHz channel spacing and the flexible grid for the LCoS is intrinsic. LCoS-based $1 \times N$ WSSs typically have ∼5 dB insertion loss and ∼35 dB extinction ratio.

Recently, a WSS approach that uses a silica-based PLC-front end and LCoS has been proposed to achieve very high port count, in particular a corresponding 1×95 WSS [81].

Liquid Crystal-on-Silicon-Based $N \times N$ WSSs $N \times N$ WSS technologies are not mature enough for industry applications but have gained much research interest. One example are LCoS-based 2×2, 3×3, and 2×4 WSSs [77, 82]. Higher port count $N \times N$ WSSs are based so far on multiple $1 \times N$ WSSs using e.g. the Spanke architecture.

It has also been suggested to use the $1 \times N$ WSS architecture shown in Fig. 10.22 for making 2×2 or 3×3 WSSs by using a more complicated LCoS phase only SLM image, which is a programmable hologram that combines multiple deflection properties for different beams [77]. However, this method cannot scale to larger $N \times N$ WSSs with $N > 3$.

Recently Han et al. demonstrated a similar 2×4 WSS based on LCoS technology [82]. Optical beams from two input ports can be simultaneously switched on a 50 GHz grid to any one of the four output ports. The 2×4 WSS demonstrated has 8 dB insertion loss, ∼25 dB isolation, it is polarization dependent, and the implementation of polarization diversity will significantly increase the overall system complexity. Based on these principles, Finisar introduced a 4×16 wavelength-selective optical switch covering the entire C-band that has a worst case 6.5 dB insertion loss [79].

10.4 Waveguide-Based Optical Switches

10.4.1 Generic Aspects

Waveguide-based optical switches enable the manipulation of light guided in interconnected planar waveguides based upon different activation mechanisms such as the electro-optic-, thermo-optic-, acousto-optic-, and the magneto-optic effect [2, 83]. There are also waveguide-based MEMS optical switches, which will be discussed in Sect. 10.5.2.2.

Waveguide-based optical switches are 2D devices, they constitute 1×2 or 2×2 switches in their own right but larger switching fabrics can also be built by cascading, and many different architectures have been proposed and realized already. The operating principle of generic planar 2×2 (or 1×2) switching structures is illustrated in Fig. 10.23 but there are quite a few other variants [2, 83].

Switching relies on the modification of the effective refractive index in one or both waveguide (WG) arms, which is accomplished by external means, in particular an applied voltage or heating, i.e. by exploiting the electro-optic- (see e.g. Chap. 8, Sect. 8.2.1.4) or the thermo-optic effect. The refractive index change introduces a phase change of the propagating wave and this modifies coupling between modes (a) or interference at the device output (b). Operation of a digital optical switch (DOS) relies on mode sorting in such a way that light propagating in the fundamental mode is directed to the arm with higher index of refraction, and the index difference required can be achieved electro- or thermo-optically [83, 84]. A DOS exhibits a step-like response once the WG asymmetry has become sufficiently large, and therefore DOSs are highly insensitive to wavelength, polarization, and other physical parameters that may normally affect device operation.

Microring resonators (MRR) are another generic element for the implementation of switches and switching matrices, and corresponding devices have been fabricated in III–V semiconductors (GaAs- and InP-based alloys) and in the SOI material system as well, and switching has been demonstrated thermo-optically [85] and by
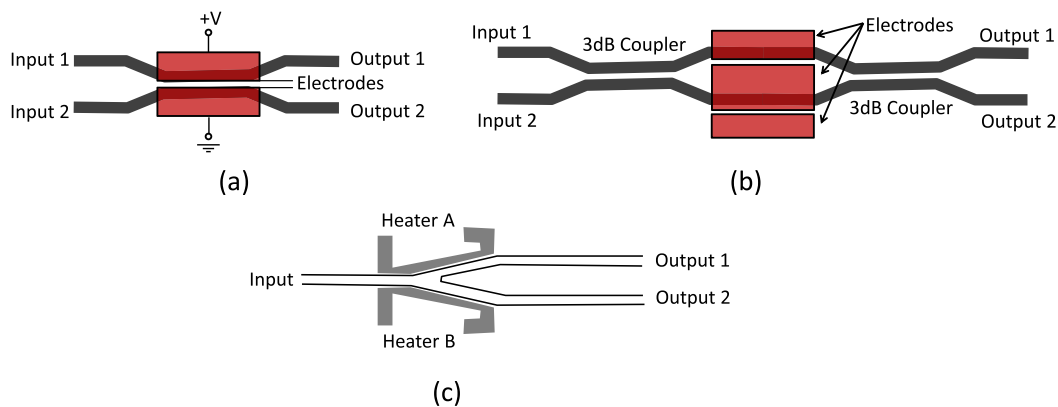

Fig. 10.23 Generic 2×2 electro-optic switch structures: (**a**) directional coupler (switch), (**b**) Mach-Zehnder interferometer switch, (**c**) digital optical switch

carrier injection also [86]. Switching based upon the resonance shift of a single MRR is of limited practical use as the resonance is rather narrow [87], but higher order MRR with multiple rings enable sufficiently broad pass bands, and an 8×4 TO switching matrix has already been demonstrated [85]. However, as it is a 2D switch architecture, the number of switching elements scales as N^2 for an $N \times N$ switch, which limits the fabrication and usefulness of larger MRR-based switching matrices. Switching power can be fairly low while the total insertion loss tends to be large due to the multi-stage cascade. A flexible-bandwidth WDM crossbar switch architecture suitable for use in high performance computing and data center applications has recently been proposed and analyzed [88]. Its capability ranges from static all-to-all wavelength connectivity to on-demand μs-scale dynamically allocated multiple-wavelength connectivity and its realization in silicon photonics is estimated to be quite feasible.

Altogether MRR-based switches have not yet achieved commercial relevance but are still in the R&D stage and will therefore not be treated in more detail in the present chapter.

10.4.2 Electro-Optic Waveguide Optical Switches

Electro-optic (EO) switches fall essentially into two categories: They either rely on the Pockels effect (see e.g. Chap. 8, Sect. 8.2.1.4), which modifies the material refractive index by an applied voltage (LiNbO$_3$, III–V semiconductors), or on carrier injection in materials without Pockels effect (Si).

10.4.2.1 LiNbO$_3$-Based Switches

LiNbO$_3$ (LN) exhibits a large electro-optic effect, high quality large wafers (>4 inch diameter) are readily available, waveguides can be fabricated by proven planar technologies (Ti diffusion or proton diffusion) [2, Chap. 2], and LN-based EO switches have been investigated and fabricated over the past 30 years [89–94].

LN-based EO switches are reliable, compact, and thermally stable. The underlying physics of EO switches offers switching times <1 ns although the capacitance of the electrodes renders this time somewhat longer in reality. Their drawbacks include relatively high insertion loss and crosstalk, and they may exhibit polarization dependence including PDL. Polarization independence is possible, but at the cost of higher driving voltage, which in turn limits the switching speed. LN EO switches are particularly attractive for high speed switching and small port counts.

Commercially available devices include 1×2, 2×2, 1×8, 1×16, and 8×8 optical switches [94]. They may have <10 ns switching time (sub-ns on request), about <4 dB insertion loss for a 1×2 or 2×2, and <5 dB for a 1×8 switch, and driving voltages are typically several volts. Crosstalk is ~18 dB, which is fairly high compared to other kinds of optical switches, however, double-stage designs can

suppress the crosstalk to better than 30 dB. 1×2 and 2×2 switches do also find application as high speed modulators and are offered with >30 GHz bandwidth, suited for 40 Gbit/s modulation [94], and polarization switches are also commercially available. Higher port count switches are generally obtained by cascading 2×2 switches, and the accumulated loss essentially limits this approach to 1×16 switches. Operation wavelengths of LN switches do typically cover the C- and the L-band.

Digital optical switches have also been realized in $LiNbO_3$ beginning with the demonstration of the concept [84] and including a 1×32 switch matrix [95] or a 4×4 switch matrix [96]. For a detailed treatment of DOSs see e.g. [97, 98].

10.4.2.2 Electro-Optic Switches in SOI

Silicon photonics [99] (silicon-on-insulator (SOI) -based photonics) enables the monolithic integration of electro-optic switches or switching matrices with digital complementary metal-oxide-semiconductor (CMOS) drivers, and this is considered particularly promising [100, 101]. As there is no Pockels effect in silicon, EO switches operate with free carrier injection. SOI-based electro-optic switches have been demonstrated with both MRR [102, 103] and MZI [104–108] architectures. MRR architecture electro-optic switches typically have narrow wavelength passband while broad wavelength band switches have been achieved with MZI structures. The power consumption of such a switch is caused by the electro-optic modulation to attain a π-phase shift, and using longer modulation arms has been verified to have lower power consumption. A 2×2 switch element exhibited 0.6 mW power consumption and 6 ns switching time [106]. Another example of a device realized in SOI is a non-blocking 4×4 electro-optic switch matrix, which exhibits fairly low (routing state dependent) power consumption in the range for various states from about 2 mW to 24 mW and 5 to 6 ns switching time, enabled by 1.2-mm-long modulation arms [108].

Typically SOI electro-optic switches have switching times comparable to that of LN-based electro-optic devices but with sub-mW power consumption only. However, these switches still suffer from high IL and low extinction ratio and may only be used for building very small port count switches. The 2D nature of the underlying switch architecture limits scalability.

10.4.3 Waveguide-Based Thermo-Optic Switches

Thermo-optic (TO) switches have been realized both, as Y-branch (DOS) and as interferometric structures in various materials [83]. The main difference between EO and TO switches is the much longer switching time of TO switches, which ranges from sub-ms to tens of ms.

10.4.3.1 Silica-Based PLC Thermo-Optic Switches based on MZI Structures

Silica-based PLCs [109, 110] have been developed for many applications and with a multitude of subcomponents, including thermo-optic switches, e.g. for building wavelength selective switches and ROADMs. One important design parameter for WGs in PLCs is the index difference Δ between core and cladding. Typically $0.5\% \leq \Delta \leq 2\%$ is used as a compromise between sufficiently low loss (the smaller Δ the better) and compact PLC design (the larger Δ the better). Table 10.1 compares properties of silica WGs for $\Delta = 0.75\%$ and $\Delta = 1.5\%$ [111].

Additional aspects of silica-based PLC technology are covered in numerous publications (see e.g. [109, 110]) and will therefore not be repeated here.

Single MZI 2×2 switches exhibit typical extinction ratios of about 25 to 35 dB. Improved optical crosstalk levels can be obtained using two cascaded MZIs for building a 2×2 cross-point switching unit (which is not a full 2×2 crossbar switch) as shown in Fig. 10.24. This double-MZI design achieves a particularly high extinction ratio in the bar-path because light power leaking from the first MZI is blocked by the second MZI in the off-state [110–114], and this property is important for matrix switches where the bar-path extinction ratio is more important than that of the cross-path [9, 111].

PLC-based thermo-optic $1 \times N$ switches and $N \times N$ switching matrices have been a research topic for many years [112–120], and $1 \times N$ thermo-optical switches have become commercially available with sizes up to 1×128, to be used e.g. for sharing a single optical channel monitor in multiple channel power monitoring. PLC-based non-blocking switching matrices with port count up to 16×16 have been made commercially available also, serving as a compact, stable, and reliable solution for the implementation of optical cross connects [118]. Characteristics of the $1 \times N$ and $N \times N$ devices include <3 dB insertion loss (or <3.5 dB for switching matrices), loss uniformity <1 dB, PDL <0.4 dB (<0.5 dB for matrices), extinction ratio >40 dB, and <3 ms switching time. Total power consumption is <4.5 W (<9 W) for a 1×8 (1×128) switch or a 8×8 (16×16) switching matrix.

Table 10.1 Properties of Silica Waveguides

Waveguides	$\Delta = 0.75\%$	$\Delta = 1.5\%$
Propagation loss	3.5 dB/m	7.9 dB/m
Fiber coupling loss	0.4 dB	2.0 dB
Minimum bend radius	5 mm	2 mm

Fig. 10.24 Basic 2×2 cross-point switching unit with double-MZI switch configuration for crosstalk reduction
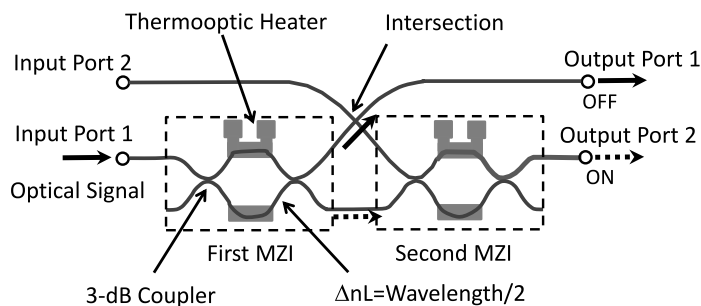
Larger switching matrices (32×32) have already been reported but are still in the R&D stage [119]. PLC-based switching matrices tend to be fairly large, e.g. a 16×16 matrix based upon WGs with $\Delta = 0.75\%$ and using double-MZI cross-point switching units has been reported to result in 100×107 mm^2 chip dimensions so that the switch (just) fits into a 6 inch wafer [111–114] while a 1×128 switch using WGs with $\Delta = 1.5\%$ has been demonstrated on a 4 inch wafer [115].

10.4.3.2 Polymer-Based PLC Thermo-Optic Switches

Polymers on silicon constitute another highly mature materials platform (besides silica or SOI). It enables the fabrication of complex PLCs including thermo-optic switches, variable optic attenuators (VOA), and power taps, but it also serves as a platform for hybrid integration of passive and active elements (see Chap. 13).

The refractive index change of amorphous polymers is predominantly due to their density change, so that a high coefficient of thermal expansion (CTE) results in a large thermo-optic effect. Enablence [122] has developed polymers with $dn/dT \approx -4 \times 10^{-4}/°$C, which is 40 times larger than the TO coefficient of silica, and 3 to 5 times larger than that of common optical polymers such as polymethyl-methacrylate (PMMA) and polycarbonate. An important benefit is that power consumption of TO switches gets the lower the higher the EO coefficient is. Furthermore, organic polymers exhibit low insertion loss ($\leq$0.1 dB/cm at all key communication wavelengths, i.e. 840 nm, 1310 nm, 1550 nm), low fiber to waveguide coupling loss ($<$0.3 dB), two orders of magnitude smaller birefringence than silica, wide controllability of refractive index contrast (maximum Δn is an order of magnitude larger than that achievable in silica), environmental stability, ease of hybridization, high yield, and low cost [122–124].

Polymer-based PLC TO switches include DOSs, a schematics of which has been shown in Fig. 10.23, and it should be added here that the angle of the Y-branch is very small, typically 0.1° [122]. The power consumption for such a switching unit (by heaters on top of the WG arms) is about 35 mW, which is much smaller than for TO switches in silica. Y-branch DOS units can be connected with bends and crossings to form $M \times N$ switching matrices, and a $1 \times N$ switch requires $(n - 1)$ 1×2 Y-branch switching units. A strictly non-blocking $N \times N$ switching matrix can be fabricated with $2N(N - 1)$ 1×2 switches using a recursive tree structure, as shown in Fig. 10.25. The total number of 1×2 DOSs needed for $N \times N$ non-blocking, recursive tree structure switches as a function of N is shown in Table 10.2.

Figure 10.26 shows a 2×2 (or cross-bar) DOS built with four 1×2 units. This switch operates in the bar state by powering the four inner electrodes while powering the four outer electrodes results in the cross state. Switch sizes from 2×2, 4×4, 8×8, to 16×16 are currently commercially available. The 8×8 cross-bar switches exhibit 40 mW power dissipation per DOS (total ~2 W), 3 dB insertion loss, and 45 dB extinction ratio, mainly limited by crosstalk at the crossings. Switching time is about 3 ms.

Fig. 10.25 Architecture of 8×8 DOS-based switching matrix based on recursive tree structure. *Each box* represents a 1×2 switch [122]
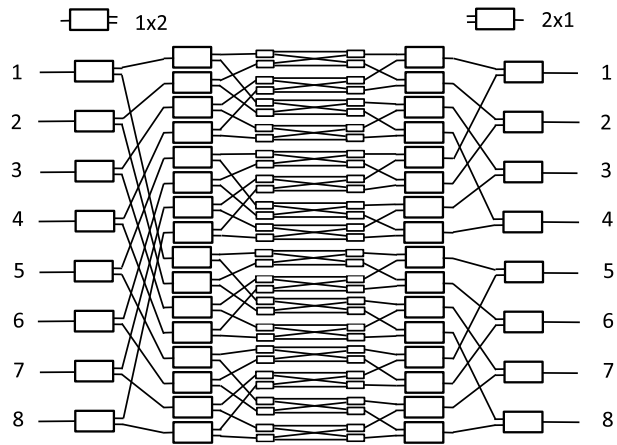
Table 10.2 Number of 1×2 switches needed in planar strictly non-blocking $N \times N$ switches using recursive tree structure [122]

N	Number of 1×2 switches
2	4
4	24
8	112
16	480
32	1,984
64	8,064
128	32,512
256	130,560
512	523,264
1024	2,095,104

Fig. 10.26 Schematic diagram of a 2×2 Y-branch digital thermo-optic switch [122]
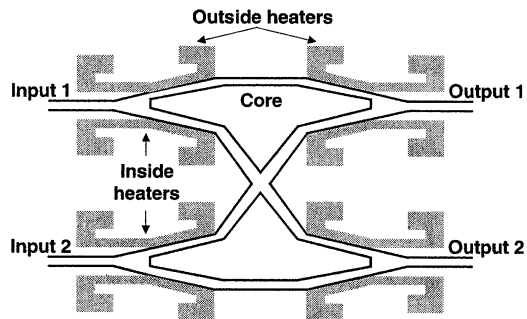
Path-independent loss $N \times N$ architectures with twice the number of 1×2 DOSs are possible in the same way as for silica-based MZI switches. However, the larger number of 1×2 switches raises power consumption and insertion loss. On the other hand, silica-based MZI 16×16 switches cannot use a recursive tree structure since the number of electrodes in combination with the much higher power consumption per switching unit will result in unacceptably high total power consumption.

Concerning power consumption of switching matrices it is worthwhile to note that a single actuation unit in silica-based technology requires about 15 times more energy than a polymer Y-branch DOS unit. On the other hand, an asymmetric MZI switching unit does not need power when in the bar (off) state. As a result the total power consumption of 8×8 switches is comparable, no matter whether they are based on a silica MZI-switch or a polymer Y-branch DOS architecture.

The largest strictly non-blocking $N \times N$ switch fabricated so far has been 16×16 [122] while significantly larger devices have been designed and are in early development stages [125]. However, due to complexity, power consumption, and limited wafer size, building matrix switches larger than 32×32 using polymer WGs is still very challenging.

10.4.3.3 SOI-Based Thermo-Optic Switches

SOI-based thermo-optic switches [126] have also found an increasing interest recently, and silicon wire-based TO switches that use the large TO coefficient of silicon can be considered very promising. Table 10.3 gives a comparison of key characteristics of silica- and SOI-based PLCs [127]. The higher refractive index of Si enables very compact devices, which is favorable for the fabrication of larger switching fabrics, the significantly higher TO coefficient is particularly useful for TO switches in general, and switching matrices ranging from 2×2 to 32×32 have been reported [128–133].

One interesting proposal has been a silicon-silica hybrid TO switch architecture that integrates low power silicon optical switches in a hybrid silica structure so that the low-loss fiber chip coupling and the long term stability of silica PLCs is combined with a silicon low power consuming optical switch [127].

10.4.3.4 Thermo-Optic Switch-Based $1 \times N$ WSS

The integration of multiple wavelength demuxes/muxes plus a $1 \times N$ switch for each wavelength results in a $1 \times N$ WSS that can be realized on a single chip, and a corresponding 1×9 WSS with 8 wavelength channels has been demonstrated in [134]. The (potential) advantages of waveguide-based $1 \times N$ WSSs include low cost and

Table 10.3 Characteristics of silica-based PLC and silicon photonics [127]

Characteristics	Silica-based PLC	Silicon photonics
Refractive index	1.45	3.4
Core size (μm × μm)	5×5	0.5×0.2
Fiber connection loss	Small	Large
Minimum bending radius (mm)	1	0.005
Thermo-optic coefficient (per °C)	1×10^{-6}	18×10^{-6}

high reliability, but with respect to narrow passband, low channel count, and insertion loss these switches are inferior to alternative solutions, and as a consequence TO switch-based $1 \times N$ WSSs have not found as widespread use as LC-based $1 \times N$ WSSs.

10.4.3.5 Thermo-Optic Switch-Based $M \times N$ Multicast Switch

An optical multicast switch (MCS) is a compact and cost-effective optical switch with colorless, directionless, and contentionless functionality, which enhances the operational flexibility of multi-degree reconfigurable optical add/drop multiplexers [135–137]. Optical MCSs combine silica- or polymer-based PLCs, TO switches and splitters/couplers, integrated on a single chip.

An $M \times N$ multicast switch comprises M $1 \times N$ splitters as input units and N $M \times 1$ switches as output units, which are interconnected in between. An $M \times N$ MCS works as an MCS for optical signals propagating from one of the M inputs to the output ports. On the other hand, if an $M \times N$ MCS is operated in the backward direction, i.e. optical signals propagate from the N output ports to the M input ports, the switch works only as a select-and-combine optical switch without multicasting function. Depending on IL and isolation specifications, different structures of $M \times N$ MCS can be utilized. Figure 10.27 shows examples of TO 8×8 MCSs (for light propagation from right to left they represent an 8×8 MCS, while they constitute a 8×8 select-and-combine switch for light propagating from the right to the left). A conventional 8×8 MCS comprises 8-arrayed 1×8 splitters or couplers and 8-arrayed 8×1 switches, and those chips are separated and connected via a 64-fiber circuit sheet in order to avoid too many waveguide crossings on a PLC chip, as shown in Fig. 10.27(a). Corresponding chips were packaged into a 240 mm $\times$ 95 mm $\times$ 12.5 mm module [135, 136]. A different circuit configuration that integrates the $1 \times M$ splitters and the TO switches into a single chip was proposed and fabricated to offer a smaller package and lower insertion loss [135, 137], as shown in Fig. 10.27(b). It should be pointed out that in references [135–137] the authors treated the 8×8 MCS as a select-and-combine switch from left to right and described it to have 8-arrayed 1×8 switches (comprising eight 1×2 switching elements cascaded serially, with a gate switch placed after each 1×2 switching element) and 8×1 combiners (comprising seven 2×1 coupler/combiner elements, placed between the stages of the switch elements). Considering signals propagating through the 8×8 MCS from right to left, the optical signal passes a 1×8 splitter and a 8×1 switch before it exits from one of the output ports. This circuit configuration reduces the maximum number of waveguide crossings by 75%, establishes an even number of crossings between the paths, and allows single chip integration of 8×8 multicast switches with 110 mm $\times$ 15 mm chip size, and a fiber pigtailed module size of 150 mm $\times$ 45 mm $\times$ 13 mm.

Optical 4×8, 8×8, 8×16, and 8×12 MCSs have been commercialized and are available from Enablence [121], Neophotonics [138] and other vendors with similar optical performance.
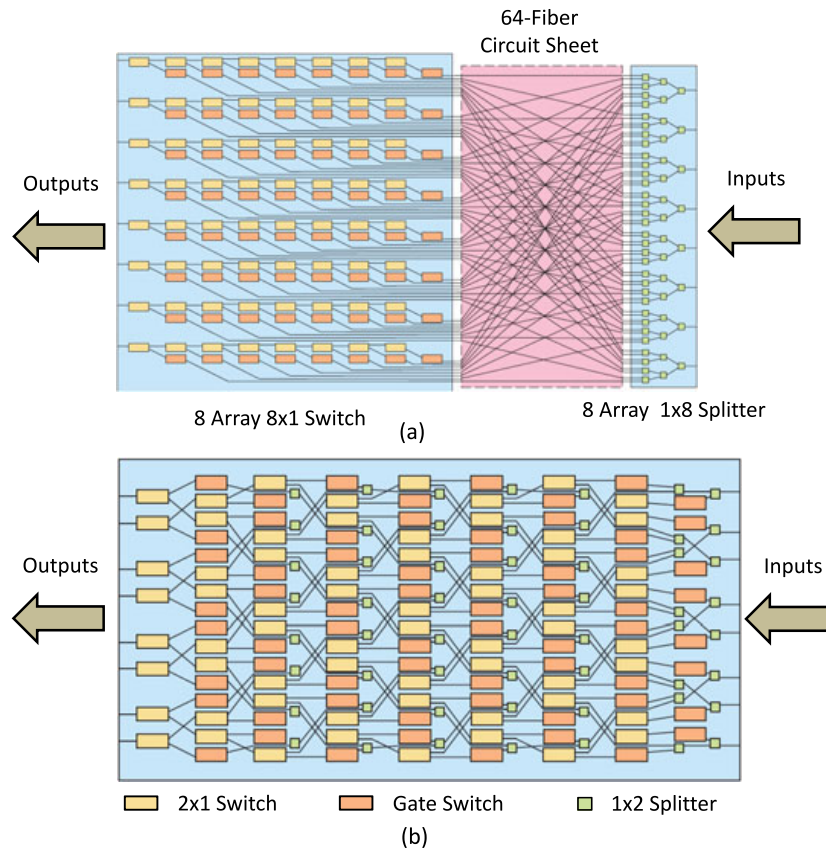
Fig. 10.27 (**a**) Conventional and (**b**) single chip circuit configuration of PLC-based multicast switch

10.5 MEMS-Based Optical Switch Technologies

10.5.1 Generic Aspects

One of the most promising technologies for optical switches with up to hundreds of ports is micro-electro-mechanical systems (MEMS) technology [139–144]. MEMS-based optical switches exhibit low loss, low crosstalk, low power consumption, small size, and reasonable speed adequate for most network reconfigurability requirements. Furthermore, MEMS fabrication techniques allow the integration of micro-optics, micro-actuators, complex micromechanical structures, and possibly microelectronics on the same substrate to realize integrated optical microsystems.

MEMS fabrication techniques utilize the mature fabrication technology of the Integrated Circuit (IC) industry. The fact that silicon is the primary substrate material used in IC circuitry and that it also exhibits excellent mechanical properties makes it the most popular micromachining material. MEMS optical switches can be fabricated using two popular micromachining technologies, surface micromachining and bulk micromachining, or a combination of both [141–143].

Bulk micromachining is the most mature and simple micromachining technology, sometimes called the etching/subtraction process as silicon is removed from

the bulk silicon substrate by etchants, anisotropic or isotropic ones. Anisotropic etchants etch different silicon orientation planes at different rates while isotropic etchants remove silicon evenly in all directions.

Surface micromachining is a more complex fabrication technique, and complex 3D mechanical structures can be created using alternate layers of sacrificial and structural materials. Free-standing 3D mechanical structures are formed by etching away the sacrificial layers. The patterned material is left as thin-film free-standing mechanical structures, suspended over the substrate according to the thickness of the etched sacrificial layer.

There are two approaches to implement MEMS optical switches: 2D and 3D MEMS switches that use digital or analogue actuators, respectively, and 2D MEMS switches can be classified into two types: 2D free-space MEMS switches and 2D MEMS waveguide switches. Furthermore, 3D MEMS can be arranged in arrays to realize multiple $1 \times N$ switches for switching individual wavelengths in WSSs.

10.5.2 2D MEMS Switches

10.5.2.1 2D MEMS Free-Space Optical Switches

2D MEMS free-space switches use digital actuators/mirrors for switching and can be used to implement 1×2, 2×2, and $N \times N$ free-space optical switches.

Figure 10.28 shows a generic schematic of a 2D switch [139, 144] with vertical reflective "digital" mirrors: They reflect a light beam by 90° if they are in the light path, while light propagates straight if the mirrors are out of the light path. One micromirror only in a column and in a row can be activated to be in the reflection position during operation. Light propagates in free space, and collimation of light coming from and going to the fibers is accomplished by micro-lens arrays.

The first 2×2 MEMS switch was reported in 1996 [145], and 1×2 and 2×2 switches were subsequently commercialized for testing, measurement, and optical protection applications [34, 145–149]. Insertion loss was <0.6 dB and some the devices had latching functionality [149].

Fig. 10.28 Schematic of 2D MEMS optical switch [139, 144]
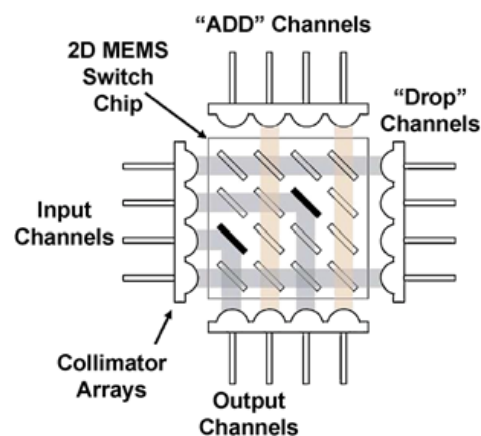
There are two basic ways for the actuation of 2D MEMS mirrors: (i) the mirrors are parallel to the substrate in the off position and, when actuated, are turned to the vertical (on) position by rotating the mirror by 90° [145, 150–152], (ii) the vertical micromirrors are moved in and out of the optical path vertically or laterally without changing the mirror angle [146, 147, 153–155]. 2D switches have been implemented by using both bulk-micromachining [145–147] and surface-micromachining technologies [150, 151, 153], and most approaches use electrostatic actuation but magnetic actuation has also been demonstrated [146, 151].

The (maximum possible) port count of free-space 2D MEMS switches is determined by various factors such as MEMS mirror size, fill factor (mirror width divided by unit cell width), mirror angle accuracy, beam spot size, and path length differences, which can be kept sufficiently small up to 64×64 switch size. Chip size may also be a limiting factor, but the main limitations for reaching large port count free-space 2D MEMS optical switches are not so much fundamental physical limits but rather related to the N^2 dependence of scalability, i.e. chip size, complexity, amount of mirrors, and control electrodes grow $\sim N^2$ for $N \times N$ port switches [156, 157]. This affects overall reliability and packaging so that the port count is essentially limited to $\sim 32 \times 32$ ports while 8×8 and 16×16 switches had become commercially available. Typical characteristics are <3.5 dB insertion loss, switching time <7 ms, crosstalk >50 dB, and PDL can be managed to be sufficiently small (<0.4 dB).

10.5.2.2 2D MEMS Waveguide Switches

2D MEMS waveguide switches use optical waveguides for beam propagation and MEMS actuators to enable switching. A corresponding solution implemented in the SOI materials platform with 50×50 ports and scaling potential to even 100×100 ports has been recently reported, a schematic and an SEM picture of the structure are shown in Fig. 10.29 [158–160].
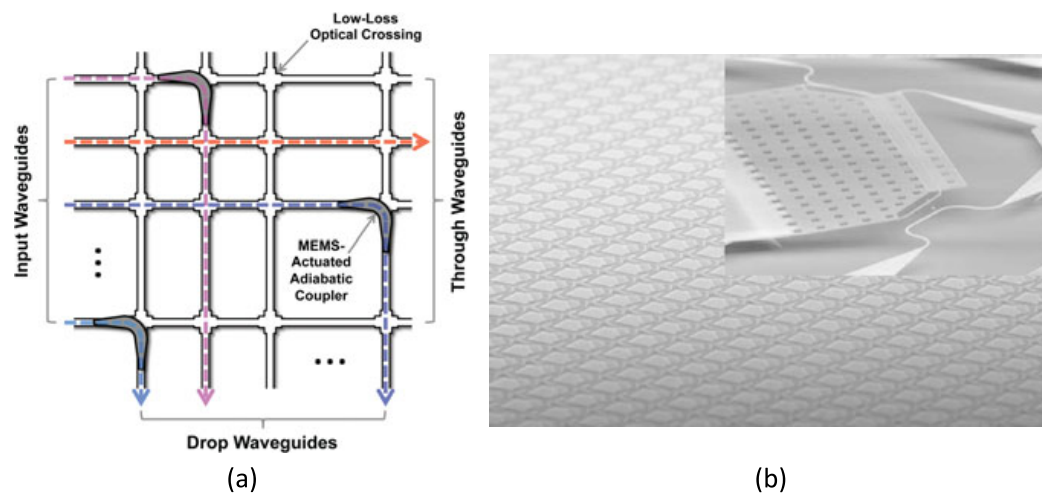

Fig. 10.29 (**a**) Schematic and (**b**) SEM picture of 2D MEMS waveguide optical switch in SOI materials platform [158–160]

The N^2 switching elements of this $N \times N$ switch are implemented as pairs of directional couplers with one arm of the directional coupler placed on a MEMS cantilever serving as activation element. In the off state the spacing between the two waveguides in the directional couplers is $>1\ \mu m$ preventing any light coupling. For the on state, the spacing is reduced to 250 nm so that light couples to the waveguide on the MEMS cantilever, is then turned by 90° through the waveguide, and finally couples back to the substrate waveguide through the second directional coupler.

The waveguides around the directional couplers have been made fully suspended by selectively etching the buried oxide and are anchored at the waveguide crossings. The size of the unit cell is $160 \times 160\ \mu m^2$, and the reported 50×50 switch with 2,500 switching elements has a chip size of $7.6 \times 7.6\ mm^2$. The insertion loss of such $N \times N$ switches is determined by the waveguide propagation loss ($\sim$0.2 dB/cm), insertion loss due to waveguide crossings (0.01 dB/crossing, number of crossing passed varies between $N-1$ and $2N-1$), and the switching element loss (measured as 0.2 dB). The reported 50×50 switch has a maximum on chip insertion loss of 9.6 dB (8.8 dB loss for propagation through 98 cells and 0.8 dB loss for switching) and high extinction ratio (>50 dB). For a 100×100 switch the total on chip loss is estimated to be 10 dB [160]. Switch response times have been measured as 0.85 μs (on) and 0.47 μs (off), the fiber coupling loss from waveguide to standard single mode fiber is ≤ 6 dB/interface, and the adiabatic coupler switch ensures broadband operation (1400 to 1700 nm wavelength range).

10.5.3 3D MEMS Switches

10.5.3.1 General Aspects

3D MEMS mirrors switch a signal from one input fiber to a selected output fiber using a pair of MEMS mirrors and fiber collimators and applying analogue beam steering, and an $N \times N$ switch requires $2N$ switching elements [160, 161]. 3D MEMS constitutes one of the most promising concepts for achieving very large switching port counts (e.g. from 32 to 2000).

10.5.3.2 3D MEMS Mirror Arrays

The key building block of 3D MEMS switches are MEMS mirror arrays, and the relevant parameters include:

MEMS Mirror Size and Fill Factor: The typical size of MEMS mirrors for large scale optical switches is in the range from 100 μm to 2 mm. The mirror matrix can have a simple or an interleaved $j \times k$ design, and the mirror reflective surface can be round, elliptical, or square. Larger mirror size and higher fill factor enable better tolerance and shorter path lengths. However, high fill factors tend to raise static and dynamic crosstalk, and making mirrors too big increases the pitch resulting in greater path lengths or the need of higher deflection angles.

MEMS Mirror Deflection Angle: 3D MEMS mirrors deflect optical beams independently in both the x- and the y-axis direction. Higher deflection angles allow shorter optical path lengths, which make the overall system more compact and less sensitive to vibrations and improve insertion loss. On the other hand, high deflection angles reduce the reflectivity and raise polarization dependent loss.

MEMS Mirror Resonance Frequency and Driving Voltages: The MEMS mirror is a mechanical resonator and has an intrinsic resonance frequency, and this is a very important characteristics as well as the Q factor. The relationship between deflection angle and driving voltage is also important in designing the driving circuit and the feedback control loop.

MEMS Mirror Reflectivity, Flatness, and Curvature: The MEMS mirror reflective surface is typically coated with a layer of aluminum or gold, resulting in high reflectivity over a wide wavelength range (92% and >95% reflectivity, respectively) from 1260 nm to 1700 nm. Flatness requirement is typically $< \lambda/10$ at 632.8 nm and the mirror curvature radius should be >0.5 m.

MEMS Stability, Angular Drift, and Control Systems: Stability of the mirror plays a critical role in the complexity of the control schemes and the reliability of the overall system. MEMS switches need to have a life time of longer than 10 years, and in order to assure low insertion loss over its life time, some sort of power monitoring and feedback control is needed but even under these circumstances the long or short term drift of MEMS deflection angles is typically required to be <0.1 degree.

Yield of MEMS Mirror Arrays: A proven concept for assuring high yield of MEMS mirror arrays comprising large numbers of mirrors is designing the mirror array with an appropriate number of spare mirrors [161].

10.5.3.3 Examples of MEMS Mirror Arrays

Surface-micromachined two-axis mirror arrays for building MEMS $N \times N$ switches with N of the order of 100s were reported in [162–164], and one early example of such a mirror that was used for the Lucent/Agere WaveStar™ LambdaRouter™ switch, is shown in a scanning electron microscope micrograph in Fig. 10.30 [162–164].

The basic element is a 500 μm-diameter round gimbal-mounted reflective mirror suspended from a fixed frame using a gimbal ring and four torsional springs, two for each axis. The MEMS mirror is attached to the ring by a second set of assemblies and can rotate with respect to the ring around a second orthogonal axis, thus achieving two degrees of freedom of tilt. The MEMS mirrors are arranged in an array with 1 mm pitch. The mirrors are tilted by applying voltages to fixed electrodes located underneath the mirror and the gimbal ring and have a mechanical deflection angle of about 6.5°. Two electrodes per axis are necessary because of the attractive nature of the electrostatic force. The electrostatic actuator is effectively a capacitor with negligible steady-state power consumption and no heat dissipation on chip, allowing for densely integrated arrays of many hundreds of micromirror devices.

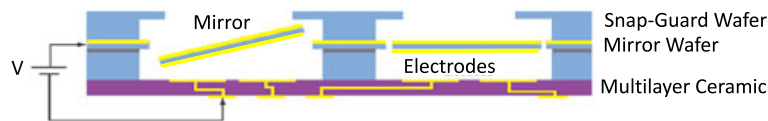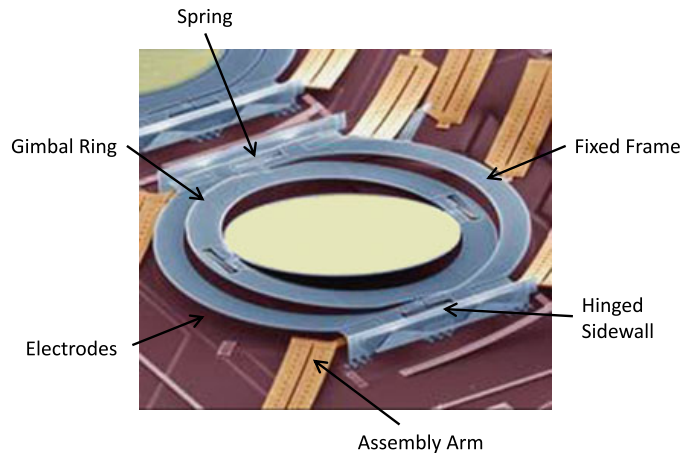**Fig. 10.30** Surface-micromachined beam-steering micromirror [163]

Fig. 10.31 Bulk-micromachined single crystal MEMS micromirror structure with simple parallel plates [165]

Another bulk-micromachined single crystal MEMS design with simple parallel plates was developed by GlimmerGlass Inc. [165]. A multilayer ceramic substrate was used for the driving electrodes, routing, and sealing, and provided the mechanical support for MEMS mirrors and drivers. The mechanical mirror structure is fabricated separately, and the two parts are bonded to form a parallel-plate electrostatic actuated 3D-MEMS mirror array, as shown in Fig. 10.31. The gimbaled mirror array was micromachined into the device layer of an SOI wafer. An SOI handling layer provided mechanical support and separation between mirrors and electrodes. The parallel plate is prone to intrinsic snap down resulting in unstable MEMS mirror operation, and in order to prevent electrostatic snap down failure, a third, snap guard layer was bonded to the top of the MEMS mirror layer, serving as a mechanical hard stop for the mirror movement. The mechanical deflection angle of these mirrors is typically <4.5°.

The other kind of MEMS mirrors use vertical comb drive actuators, also based on electrostatic actuation, was first reported in [166], and [167], and several variations of vertical comb drive mirrors have been reported subsequently, including self-aligned vertical combs, angular vertical combs, electrostatically assembled vertical combs, and thick vertical combs (100 μm) attached to mirror edges on double sided SOI wafers [167–174]. Bulk micromachined micromirrors with vertical comb drive actuators do not have the snap-down failure effect, which increases both the stability of such MEMS structures and the actual deflection angles. In addition, compared to parallel plate structures, micromirrors with vertical comb drive offer much larger torques so that the operating voltage can be smaller and the resonance frequency can

be higher. At the same time vertical comb drive offers much higher deflection angles, which is particularly advantageous for 3D MEMS switch applications. Calient has been using vertical comb drive actuators to fabricate 2-axis MEMS mirror arrays reliably since 2000 with mirrors having high mechanical deflection angles of more than 20° [175, 176].

10.5.3.4 2D High Port Count High Precision Fiber Collimator Arrays

Fiber collimator arrays containing an array of optical fibers and a corresponding array of micro-lenses constitute another key element of 3D MEMS-based switches. An important characteristics of fiber collimator arrays is their beam pointing error, which has been confirmed to be <1 mrad for 98% of the beams, and this can be achieved if the fiber position accuracy is ±1 μm and the micro-lens pitch error and focal length variations of the micro-lens array are sufficiently small: A wave front aberration of a tenth of a wavelength may cause the path to have observable IL penalty already.

Micro-lens arrays need to be monolithically integrated and can be manufactured in high volume. So far refractive micro-lenses are the best choice for large port count MEMS optical switches since they offer low loss performance over a broad wavelength range. In contrast, diffractive lenses have high chromatic aberration that causes high wavelength-dependent loss so that they should be used for narrowband designs only. Both silicon and glass micro-lenses can be used for the telecom wavelength range (1260 nm–1650 nm). The lens shape is typically spherical, and for the same insertion loss target, lens shape accuracy requirements vary for different materials as a function of refractive index. For example, comparable radius curvature non-uniformity causes much more focal length variations for glass than for silicon lenses. The lens shape accuracy and the radius of curvature uniformity specifications for glass lenses are 5 times higher than those for silicon lenses so that silicon micro-lens arrays [179] are better suited for the applications under consideration here. A ±1% focal length uniformity over the complete lens array guarantees sufficiently uniform optical spot sizes, and a pair of fiber collimator arrays will typically have about 0.4 to 0.6 dB IL.

10.5.4 3D MEMS N × N Optical Switches

10.5.4.1 3D MEMS Switch Architectures, General Aspects

Various 3D MEMS optical switch architectures have been proposed and realized during the past 20 years with different switch port count, mirror deflection angle, pitch, fill factor, MEMS mirror stability, path-length, total packaging size, and optical performance such as insertion loss and crosstalk. For all these architectures, the input and output fibers are either arranged in the same or in two fiber collimator
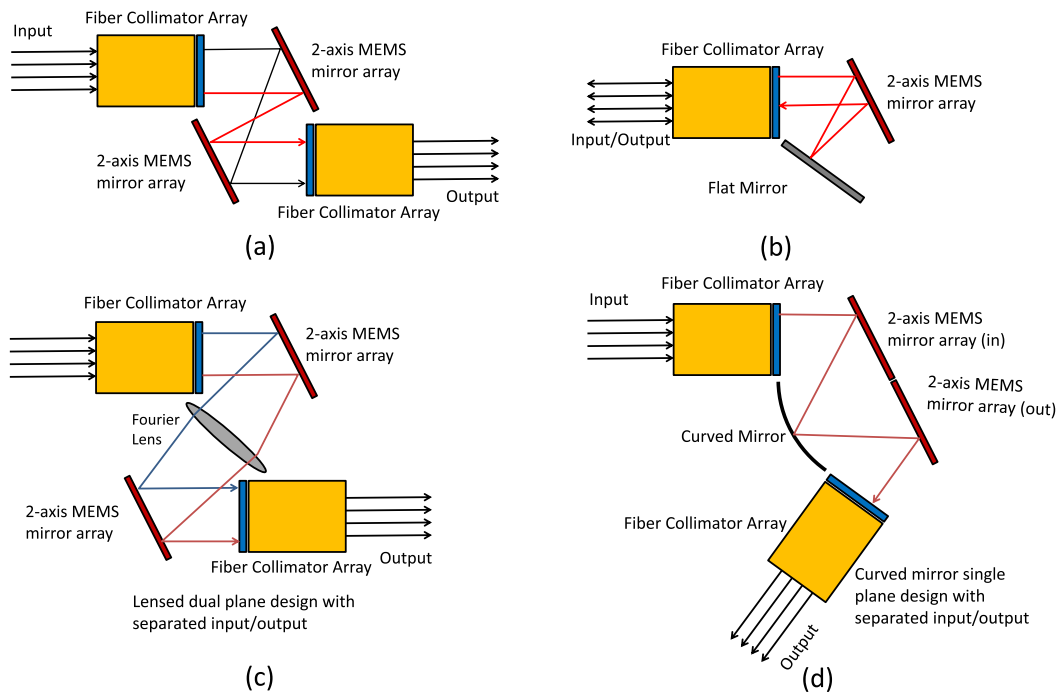
Fig. 10.32 Different 3D MEMS switch architectures, (**a**) parallel dual plane design [162, 163, 175], (**b**) flat mirror single plane design [165], (**c**) dual plane design with separated input/output and Fourier lens [184–186], (**d**) curved mirror single plane design with separated input/output [182]

2D array(s), and the optical beams are steered in three dimensions by two stages of 2-axis micromirrors. The two MEMS mirror arrays (for both, inputs and outputs) can be in one chip or in two chips.

The most relevant designs are:

(a) Parallel dual plane design [162, 163, 175], as shown in Fig. 10.32(a)
(b) Flat mirror single plane design [165] that uses a fiber collimator array that has both inputs and outputs (Fig. 10.32(b))
(c) Dual plane design with separated input/output and Fourier lens [184–186] (Fig. 10.32(c))
(d) Curved mirror single plane design with separated input/output [182] (Fig. 10.32(d))
(e) Roof-type mirror single plane design [189]
(f) 4F design with separated input/output [187]

Four examples of the architectures are shown in Fig. 10.32. The parallel dual plane design, as illustrated in Fig. 10.32(a), constitutes one of the most important and widely used structures [161–163], and the Calient switch as well as various implementations by Lucent Technologies, discussed in more detail below, are based upon this design. It has been demonstrated that optical switches with port count up to thousands are possible with this architecture, however, larger maximum deflection angles are required in order to keep the path lengths short [198, 199].

10.5.4.2 Calient 3D MEMS Switches

Calient developed a 384 × 384 non-blocking optical switch with very good optical performance based on the configuration shown in Fig. 10.32(a) [175, 176]. Due to the symmetrical design, both input and output mirrors require the same maximum deflection angles (up to ±20°). The MEMS array is shown in Fig. 10.33(a). The typical relationship between the driving voltage and the mechanical deflection angle is shown in Fig. 10.33(b). The optical path length is 46 mm to 55 mm, with an average mirror-mirror separation of 26.9 mm.

Large scale optical switches with 3D MEMS mirrors generally need a feedback control system so that time and/or temperature dependent variations of (a) MEMS deflection angles (b) high voltage driver output voltages, and (c) mechanical alignments can be compensated by fine-tuning the MEMS mirrors.

Switch feedback control can be implemented either as a direct or an indirect monitoring system, and direct monitoring can be implemented in several ways, e.g. using the customer input light and tap couplers or internal light of an un-used band and wavelength division multiplexing. A 3D MEMS optical switch architecture with direct power monitoring (similar to the one used by Calient) is shown in Fig. 10.34. Each input/output fiber has a 1 × 2 beam splitting coupler to tap a small portion of the power, which enables the switch path insertion loss to be measured.

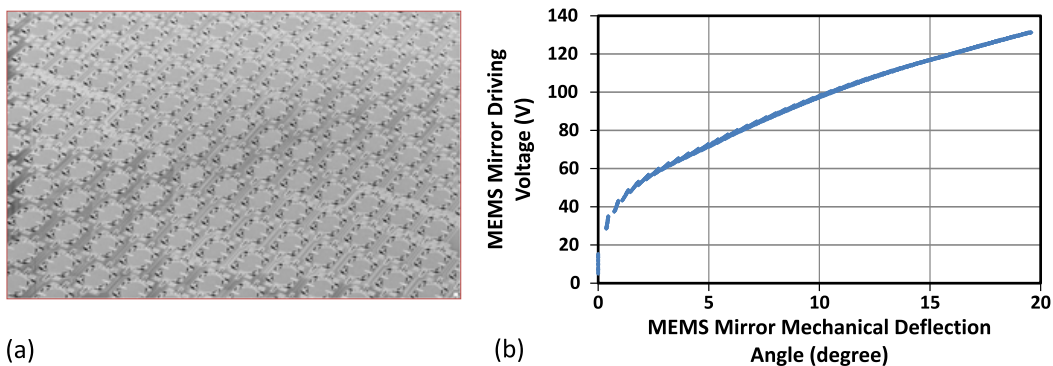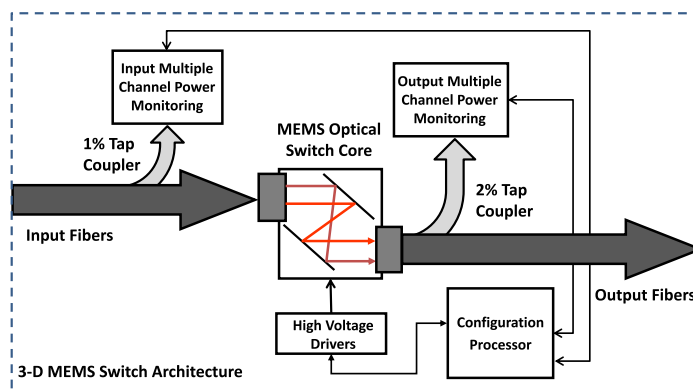(a)   (b)

Fig. 10.33 (**a**) 400 mirror 3D MEMS array, (**b**) relationship between driving voltage and mechanical deflection angle for MEMS mirrors as shown in (**a**)

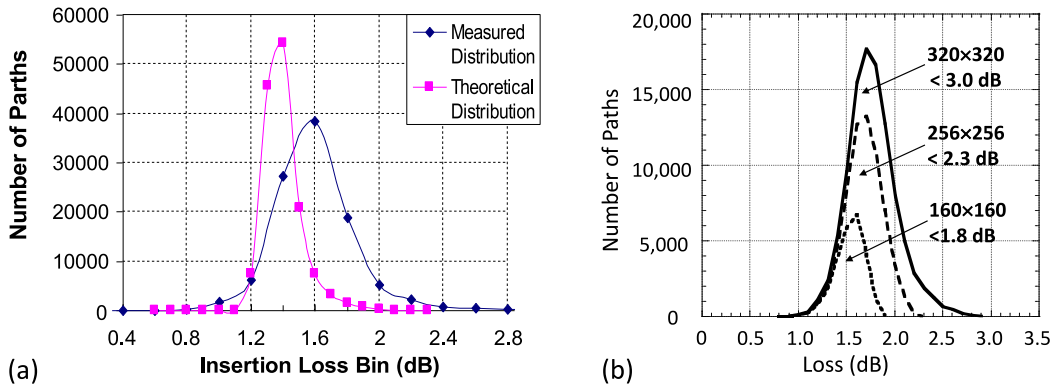**Fig. 10.34** 3D MEMS switch system architecture with optical power monitoring functions

Fig. 10.35 Insertion loss performance of Calient 3D MEMS switch. (**a**) Theoretical and measured insertion loss distribution for a 360×360 switch, (**b**) insertion loss distribution for different switch sizes, all data for 1.55 μm

The insertion loss for each path of an optical switch can be calculated by using fiber collimator measurement data and taking the optical configuration into account. Calculated and measured overall system insertion loss values at 1550 nm for all 129,600 paths of a 360×360 optical switch are shown in Fig. 10.35(a). The measured overall system insertion loss includes switch core loss and loss of connectors and the power monitoring unit. Compared to the modeling the experimentally determined loss is slightly higher and has a wider distribution, which is partly due to connector variations. Furthermore, insertion loss increases as the port counts gets larger as shown in Fig. 10.35(b), where the measured insertion loss from an actual switch is shown for different port counts.

The wavelength dependent loss variation for the O-, S-, C-, and L-bands are very small (<0.8 dB), with 1550 nm insertion loss typically larger than loss at 1310 nm (in agreement with theoretical calculations). The E-band exhibits about 1 dB additional wavelength dependent loss due to the water peak of the fiber couplers. This peak can be removed by using water-peak removed fiber couplers.

Other critical optical parameters of 3D MEMS switches are return loss, directivity, polarization dependent loss, crosstalk, and switching time. The return loss is dominated by the return loss of the fiber collimators, and measured values vary from 42 dB to 55 dB with typical values of 46 dB. The directivity is about 70 dB. Different paths of a switch have different PDL, measured values are <0.2 dB and typical PDL is 0.05 dB.

Static crosstalk is measured to be better than 60 dB and it is primarily due to adjacent ports while non-neighboring ports have typically 80 dB static crosstalk. Dynamic crosstalk occurs only when a new connection is set up, and worst values observed during beam scanning amount to 30 dB. Switching time for Calient MEMS switches is <50 ms. The resonance frequencies of the MEMS mirrors are of the order of 400 to 600 Hz. Moving the mirrors too rapidly excites the resonant mode of the mirror and causes ringing of the optical signal, but a special voltage or driving profile to control the movement of MEMS mirrors assures low ringing of the optical signal and fast switching time. The feedback control of the 3D MEMS switches

may cause signal fluctuations during active control cycles and therefore the MEMS mirror movement steps have to be carefully chosen in order to ensure small optical signal fluctuations.

Finally it should be mentioned that the Calient 3D MEMS switch discussed so far can be scaled to more than 1000×1000 ports with reasonably low optical insertion loss with the same kind of MEMS mirrors and similar optical design [177].

10.5.4.3 Miscellaneous 3D MEMS Switches

Glimmerglass 3D MEMS Switches   The flat mirror single plane design developed by Glimmerglass and illustrated in Fig. 10.32(b) [165, 178] uses a fiber collimator array that has both input and output ports and a MEMS mirror array in a single plane, serving as both input and output MEMS mirrors. A flat mirror reflects the optical paths back to the MEMS mirror array. In this design, any port can be used as input or output port, any port can be switched to any port, and a non-symmetric number of input and output ports is possible. For example, if the total switch has 192 mirrors, the switch size can be 1×191, 96×96, 32×160, etc. as long as the input port count and output port count make the total amount of 192. Glimmerglass offers a 96×96 switch based upon the flat mirror single plane design (Fig. 10.32(a)) and uses a dual plane design for its 192×192 3D MEMS switch (Fig. 10.32(c)). The switch uses bulk-micromachined parallel plate beam-steering micromirrors (see Fig. 10.31) with about $<4°$ deflection angle [165]. The 192×192 switch has a typical (maximum) insertion loss of 1.7 (3.7) dB, 20 ms switching time, 70 dB crosstalk, and offers direct optical power monitoring and feedback control loops.

Fujitsu 80 × 80 Switch   Fujitsu has proposed and implemented a roof-type mirror single plane design for an 80×80 switch, which uses two-axis tilt comb-driven 2D MEMS mirror arrays with V-shaped torsion bars for the 3D MEMS switch [188]. The MEMS mirrors have maximum deflection angles of $\pm 5°$. Mean insertion loss amounts to 2.6 dB with a variation from 1.5 to 4.0 dB. Another characteristic feature is the fact that input and output ports are pre-assigned [189].

Lucent Technologies 3D MEMS Switches   Lucent Technologies has reported 3D MEMS switches with different architectures, and the 3D MEMS switch commercialized first was the "LambdaRouter" using the parallel dual plane design (see Fig. 10.30 and Fig. 10.32(a)) [162–164, 180, 181]. The low deflection angles of the MEMS mirrors used resulted in long optical paths and high insertion loss.

Lucent also demonstrated 238×238, 256×256, and 1100×1100 3D MEMS switches using a lensed dual plane design, i.e. a structure with a Fourier lens between the two MEMS mirrors [184–186] (see Fig. 10.32(c)). The Fourier lens enables lower total insertion loss even if low deflection angles of the MEMS mirror array (about $5°$ mechanical deflection angle on both axes) are used. The 238×238 switch exhibited 1.33 dB mean insertion loss with a loss variation from 0.8 dB to

2 dB [184] while a mean fiber-to-fiber insertion loss of 2.1 dB and maximum insertion loss of 4.0 dB across all possible connections were reported for the 1100×1100 switch [186]. This is the largest 3D MEMS switch demonstrated so far and clearly demonstrates the potential of the Fourier lens in improving the insertion loss.

The 4F design with separated input/output is another concept developed by Lucent Technologies and implemented for a 100×100 switch [187]. Its key features are two 4F imaging systems, which make the design rather complex. It has been demonstrated that the 4 F imaging system is more than ten times less sensitive to microlens-to-fiber misalignment, however, the insertion loss (2.9 dB mean, variation from 1.4 to 4.5 dB) is higher than observed for switches using similar MEMS mirrors with comparable port count but alternative design. Altogether the performance of these switches did not meet expectation and the concept does not appear to be particularly promising.

In general Lucent Technologies MEMS switches include integrated power monitoring for each fiber and feedback control [183], however, switch systems with open-loop control were also reported [184].

NTT MEMS Switch NTT fabricated silicon single crystal 1024 channel parallel plate MEMS mirrors for 3D MEMS switch applications [190], and also developed a 100×100 switch and a fully functional 128×128 switching system with mean loss of 2.6 dB and insertion loss variations from 0.6 to 4.8 dB [191–193]. NTT also demonstrated a 512×512 optical switch based upon a curved mirror design that also has two separated MEMS planes with separated inputs/outputs. The design exhibits characteristics essentially similar to that of the design with flat mirror but offers reduced deflection angles and smaller beam spot size on the mirrors, which improves clipping loss. The 512×512 switch exhibited a mean insertion loss of ~5 to 6 dB and variations from 2 to 11 dB [194].

3D MEMS Switch with Indirect Monitoring An interesting variant of the 3D MEMS architecture that uses the flat mirror single plane design and indirect optical monitoring was proposed and demonstrated in [195]. The goal of the architecture is to offer a cost effective feedback loop to control MEMS mirror movement without directly monitoring the optical power inside an optical fiber. Out-of-band light is injected along each of the beam paths and imaging sensors are used to monitor the beams deflected from the MEMS mirrors so that the mirror position can be monitored and direct feedback control for the MEMS mirrors is possible. The advantages of this indirect optical monitoring include compact design with dark fiber connection ability. The feedback control system can track and correct MEMS mirror drift and driver voltage drift, however, it cannot track mechanical structure changes of the many optical components, so that the optimized position from the feedback control system may not be the best position for the switch to have lowest insertion loss. Since the optical power from the fibers is not directly monitored, the feedback control system may have tracking errors.

Concluding Remark There are other approaches that seek to build modular MEMS optical switches [196], which do not use monolithic but smaller MEMS

mirror chips in a modular way so that the switch size can be enlarged by adding switching modules.

The Clos architecture can be used for the implementation of much larger port counts, however, due to the three stage switching architecture, insertion loss increases considerably.

Altogether, MEMS optical switches have matured in the past, commercial products have become available, and MEMS optical switches have been deployed for lab automation, telecom applications, and recently in data centers. Scaling 3D MEMS optical switches from about 360×360, which represents the current state-of-the-art (see, however, the section on Lucent switches above), to extreme large port counts in the range of several thousands is possible and corresponding research and development is ongoing [197–199].

10.5.5 3D MEMS-Based Wavelength Selective Switches

#### 10.5.5.1 3D MEMS-Based 1 × N Wavelength Selective Switches

The first MEMS-based WSS built was a wavelength blocker for an ROADM, which is a 1×1 WSS [200–205]. Wavelength blockers use a 1D array of MEMS mirrors with one axis of deflection to achieve the attenuation/blocking function on each wavelength channel. A wavelength blocker is simpler than a $1 \times N$ WSS, but the basic principle is the same.

A 3D MEMS-based $1 \times N$ WSS can be designed according to the generic illustration in Fig. 10.4 (with a 3D MEMS mirror array with multiple mirrors in a 1D array taken as optical switching element) [206–211]. Incoming light is angularly separated by the transmission grating, a collimating lens transfers the angularly dispersed wavelengths to different MEMS mirrors which can pivot in both x- and y-directions, and redirect each wavelength slice to the corresponding output port through the diffraction grating.

For hitless operation, the 2-axis MEMS mirror movements have to follow a special pattern to avoid unwanted leakage. Sometimes one axis is used for switching only and the other is used for switching and attenuation. Wavelength selective switches should be compact so that the package fits into a blade space of a telecom rack, and reflective grating-based $1 \times N$ WSS designs are favorable in this respect as reflective gratings fold the optical light path resulting in compact design. A corresponding 1×4 WSS was demonstrated by Lucent Technologies [207], and Wu et al. reported a 1×32 WSS [208–211].

The WSSs reported in [207–211] have circular optical beams. However, since the MEMS mirrors can be rectangular or elliptical, the optical beam must not necessarily be circular. If the beam is elliptical and the long direction is aligned to the grating dispersion direction, a better wavelength resolution can be achieved while the short extension in the other direction keeps the height of the optics small.

Fig. 10.36 $1 \times N$ WSS schematic using elliptical beams. (**a**) Schematic optical setup of $1 \times N$ WSS with cylindrical lens and cylindrical reflective mirror, (**b**) schematic optical setup of a 1×43 WSS with anamorphic prism pair [213]
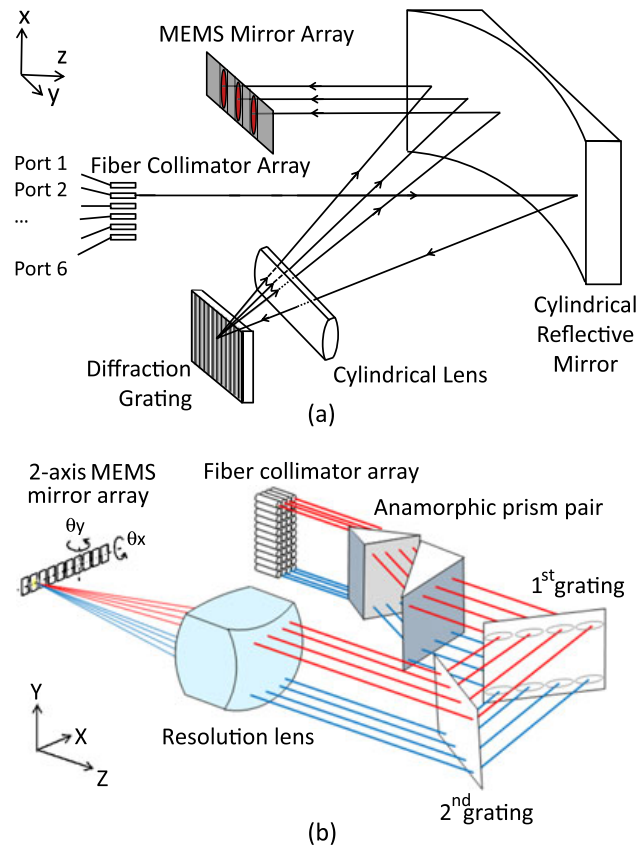
Two corresponding architectures have been proposed already, one of them using a cylindrical lens and a cylindrical reflector (see Fig. 10.36(a)), the other one using an anamorphic prism pair (see Fig. 10.36(b)). In Fig. 10.36(a), the reflective grating is used to disperse different wavelength beams to different MEMS mirrors in the wavelength dispersive plane while the cylindrical lens combines the beams in the switching plane. This way the beam in the x-direction is much bigger than in the y-direction on the MEMS mirrors, and the beams in y-direction are much larger than in x-direction on the diffractive grating surface. This architecture is used to build many commercially available $1 \times N$ WSSs [212]. In Fig. 10.36(b), the same principal was implemented by an anamorphic prism pair. Based on this architecture, a 1×43 WSS with 40 channels at 100 GHz channel spacing was demonstrated [213].

The performance of the MEMS micromirror array has a significant influence on the performance of the WSS [214]. Micromirror arrays used in $1 \times N$ WSSs include electro-magnetic or electrostatic actuations. The most important parameters are high deflection angles, high fill factor, low angle drift, mirror size, and pitch to match the grating dispersion. Most mirror arrays have a pitch of about 100 μm with a fill factor of >98%. The total mirror number in a row is typically the same as the channel number. However, in order to enable flexible passbands, a larger number of mirrors (e.g. twice the channel number or even more) is needed, and that makes the design of corresponding $1 \times N$ WSSs difficult as flexible passbands require smaller pitch and larger numbers of MEMS mirrors to be actuated.

10.5.5.2 3D MEMS-Based $N \times N$ Wavelength Selective Switches

Making $N \times N$ WSSs is a very challenging task. $N \times N$ WSSs have $N \times m$ MEMS mirrors where m is the total wavelength channel number. For an 8×8 WSS with 40 channels, each MEMS array has 320 mirrors. Furthermore, 100% MEMS mirror yield is required, the MEMS mirror size is very small, it should have >92% fill factor, and should be arranged in a 2D array with about 10 degree deflection angle, which is also challenging.

The majority of $N \times N$ WSSs are constructed with multiple $1 \times N$ WSSs in a Spanke configuration, and due to the availability, reliability, and modularity of $1 \times N$ WSSs such $N \times N$ WSSs have been widely used in ROADMs.

However, there is research directed toward building integrated $N \times N$ MEMS WSSs. One example of an $N \times N$ all optical wavelength selective optical cross-connect switch architecture was proposed by O. Solgaard et al. [20]. This approach uses an array of MEMS mirrors for the full functionality of $N \times N$ port optical wavelength switching. It requires two MEMS mirror arrays to steer different wavelengths to different ports, and the wavelength selective routing apparatus uses a diffraction grating to separate the multi-wavelength signals to individual wavelength channels.

Another concept to build an $N \times N$ WSS has been proposed and demonstrated by integrating AWG devices with MEMS mirrors [215–217], which resulted in particularly narrow passbands [217].

More recently, an experimental 5×5 WSS with 46 wavelength channels and 100 GHz spacing has been demonstrated [218]. The two MEMS arrays used as switching engines are composed of 46×5 micromirror arrays monolithically integrated on each MEMS chip. The reported insertion loss is 35 dB with a 15 dB extinction ratio.

A 4×4 WSS for 8 CWDM wavelength channels using a monolithic SOI chip comprising four 4×1 MEMS wavelength-selective switches and four 1×4 passive splitters, together with a 4×4 waveguide shuffle network is another reported approach [219]. An 8-element micromirror array matching the CWDM (1470 to 1610 nm) grid with 20-nm spacing was integrated in the waveguide, and the MEMS mirror is actuated by a rotary comb-drive actuator. The demonstrated 4×4 WSS has 24 dB insertion loss with 25 dB crosstalk.

All experimentally demonstrated $N \times N$ WSSs discussed above have very high loss, and significant additional effort is needed in order to make these $N \times N$ WSSs suited for system applications.

An alternative approach to build an $N \times N$ WSS is to use individual wavelength demux/mux and a large port count optical switch to integrate them together. Using Calient's S320 320×320 switch, 8 demux and 8 mux, an 8×8 WSS with 40 channels and 100 GHz channel spacing has been implemented [220]. The WSS had about 11 dB total IL and is a low cost solution. The drawback is the narrow passband due to cascading individual mux and demux.

10.6 Piezoelectric Optical Switches

Other variants of optical switches include piezoelectrically actuated optical switches developed by Polatis [221–224]. Unlike 3D MEMS mirrors, the piezoelectric actuators are used as the switching elements that steer the optical beams in free space from input ports to output ports.

Two approaches for piezoelectric-actuator-based $N \times N$ switches have been implemented by Polatis. One approach uses piezoelectric-actuators for moving the tip of the fiber to steer the beam, as shown in Fig. 10.37. The lateral movement in x- and y-direction is translated to the deflection angle of the optical beam through a lens. Each fiber is associated with a lens for this purpose. The lens also collimates the light signal from the fiber to a collimated beam. The optical signal passes directly from the input to the output fibers in free space through two lenses. The design of the switch is highly depending on how small the fiber/actuator assembly and the maximum displacement of the piezoelectric actuator are. An alternative approach uses a piezoelectric actuator to move a fiber collimator assembly as a whole unit and making the connection [221–224].

Comparing the two approaches shows that moving fibers requires smaller displacement while the loss is higher since the fiber is off the center of the lens, which causes aberration induced insertion loss.

Polatis offers optical switches based on piezoelectric beam steering technology from 4×4 to 192×192, with a recent announcement of 384×384 switches. The ad-

Fig. 10.37 Schematic of piezoelectric $N \times N$ optical switch [221–224]
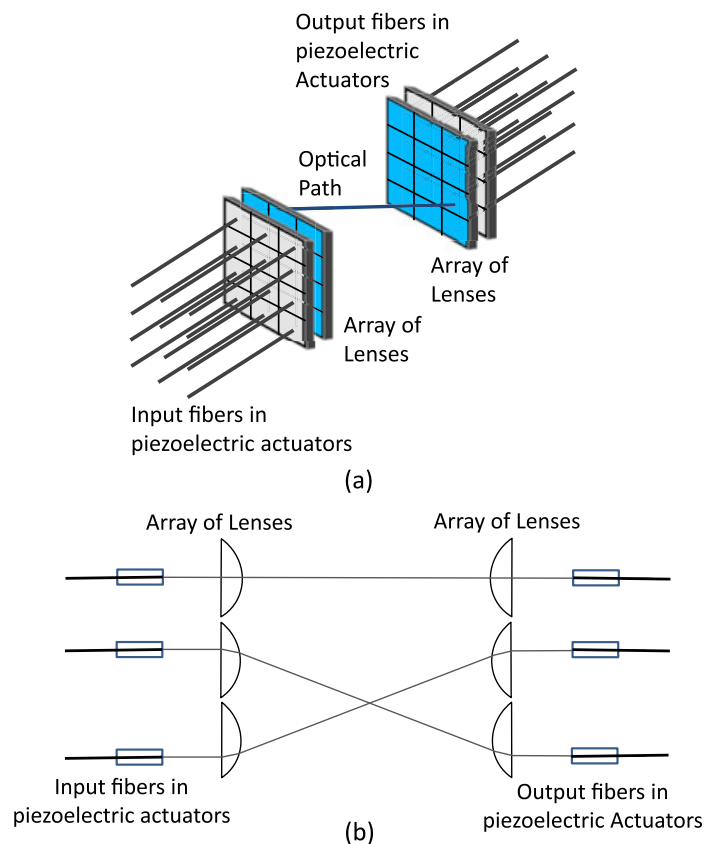
vantages of these switches are their low insertion loss (minimum 0.4 dB, worst case 2.8 dB not including connectors), modularity, and insertion loss stability. Disadvantages include higher cost and difficulties in packaging density and displacement of the piezoelectric elements.

10.7 Summary and Outlook

Optical switches continue to improve in performance with lower loss, lower back-reflection, better spectral characteristics. Integration continues to expand, resulting in lower cost, smaller size and higher reliability. Telecom and datacom networks continue to increase in capacity, which drives the demand for high capacity optical switching rather than electrical switching. The integration of optical amplifiers allows such switching networks to scale to larger sizes, although with some drawbacks. The optimum switch architecture depends on the application, and consequently, a wide range of switch technologies and architectures continue to be researched and commercialized.

References

1. R. Ramaswami, K. Sivarajan, *Optical Networks: A Practical Perspective* (Morgan Kaufmann, New York, 1998)
2. T.S. El-Bawab, *Optical Switching* (Springer, New York, 2006)
3. G.I. Papadimitriou, C. Papazoglou, A.S. Pomportsis, *Optical Switching* (Wiley-Interscience, Hoboken, 2007)
4. C. Li, *Principles of All-Optical Switching* (Wiley/Science Press, Beijing, 2015)
5. G.A. Fish, B. Mason, L.A. Coldren, S.P. DenBaars, Compact, 4×4 InGaAsP–InP optical crossconnect with a scaleable architecture. IEEE Photonics Technol. Lett. **10**(9), 1256–1258 (1998)
6. Generic requirements for singlemode fiber optic switch, Telcordia Technologies Generic Requirements, GR-1073-Core (Piscataway, NJ, 2011)
7. T. Shimoe, K. Hajikano, K. Murakami, Path-independent insertion loss optical space switch, in *Opt. Fiber Commun. Conf.* (OFC'87), Reno, NV, USA (1987), Techn. Digest, paper WB2
8. T. Nishi, T. Yamamoto, S. Kuroyanagi, A polarization-controlled free-space photonic switch based on a PI-loss switch. IEEE Photonics Technol. Lett. **5**, 1104–1106 (1993)
9. K. Padmanabhan, A.N. Netravali, Dilated networks for photonic switching. IEEE Trans. Commun. **COM-35**(12), 1357–1365 (1987)
10. R.A. Spanke, Architectures for large nonblocking optical space switches. IEEE J. Quantum Electron. **QE-22**(6), 964–967 (1986)
11. C. Clos, A study of non-blocking switching networks. Bell Syst. Tech. J. **32**, 406–424 (1953)
12. M.L. Heitner, J.J. Song, R. Vianna, Folded Clos architecture switching, US patent number 6696917 (2000)
13. W.T. Anderson, J. Jackel, G.K. Chang, H. Dai, W. Xin, M. Goodman, C. Allyn, M. Alvarez, O. Clarke, A. Gottlieb, F. Kleytman, J. Morreale, V. Nichols, A. Tzathas, R. Vora, L. Mercer, H. Dardy, E. Renaud, L. Williard, J. Perreault, R. McFarland, T. Gibbons, The MONET project-a final report. J. Lightwave Technol. **18**(12), 1988–2009 (2000)

14. K.S. Jepsen, U. Gliese, B.R. Hemenway, S. Yuan, K.S. Cheng, J.E. Hurley, L. Guiziou, J.W. McCamy, N. Boos, D.J. Tebben, B. Dingel, M.J. Li, S. Gray, G.E. Kohnke, L. Jiang, V. Srikant, A.F. Evans, J.M. Jouanno, Network demonstration of $32\lambda \times 10$ Gb/s across 6 nodes of 640×640 WSXCs with 750 km Raman-amplified fiber, in *Opt. Fiber Commun. Conf.* (OFC'2000), Baltimore, MD, USA (2000), Techn. Digest, paper PD35

15. M. Adams, ROADM and wavelength selective switches perspectives for fiber optic manufacturing test engineering, JDSU Technical White Paper (2008)

16. Finisar Corporation, Wavelength selective switches for ROADM applications, Finisar Corporation WSS ROADM Product Guide (2011)

17. P. Wall, P. Colbourne, C. Reimer, S. McLaughlin, WSS switching engine technologies, in *Opt. Fiber Commun. Conf. and Nat. Fiber Opt. Eng. Conf.* (OFC/NFOEC'08), San Diego, CA, USA (2008), Techn. Digest, paper OWC1

18. E.G. Loewen, E. Popov, *Diffraction Gratings and Applications* (Marcel Dekker, New York, 1997)

19. J.L. Wagener, T.A. Strasser, Multiple function digital optical switch, US Patent No. 8,086,080 (2011)

20. O. Solgaard, J.P. Heritage, A.R. Bhattarai, Multi-wavelength cross-connect optical switch, US Patent 6,374,008 (2002)

21. Calient Technologies, S-320 optical circuit switch datasheet. http://www.calient.net/products/s-series-photonic-switch/ (2013)

22. B.C. Collings, Advanced ROADM technology and architecture, in *Opt. Fiber Commun. Conf.* (OFC'15), Los Angeles, CA, USA (2015), Techn. Digest, paper Tu3D.3

23. www.enablence.com, Enablence technologies, Inc., iMS™ $M \times N$ Multicast switch modules (2010)

24. P.G. Hale, R. Kompfner, Mechanical optical fibre switch. Electron. Lett. **12**(15), 388 (1976)

25. W.J. Tomlinson, Application of GRIN-rod lenses in optical fiber communication systems. Appl. Opt. **19**, 1127–1138 (1980)

26. SELFOC Product Guide, manufacturer's literature on fiber collimators, NSG America Inc., NJ, USA (1997)

27. CASIX Inc, Technical specifications for C-lens. http://www.casix.com/products/glass-optics/telecom-optics/c-lens.shtml

28. S. Yuan, N.A. Riza, General formula for coupling-loss characterization of single-mode fiber collimators by use of gradient-index rod lenses. Appl. Opt. **38**, 3214–3222 (1999)

29. D. Marcuse, Loss analysis of single-mode fiber splices. Bell Syst. Tech. J. **56**, 703–719 (1977)

30. H. Kogelnik, Coupling and conversion coefficients for optical modes, in *Proceed. Symp. Quasi-Optics*, ed. by J. Fox. Polytechnic Brooklyn, Brooklyn, NY, USA. Polytechnic Institute Microwave Research Institute Symposia Series, vol. 14, pp. 335–347 (1964)

31. www.senko.com, Senko advanced components, fiber array and V-groove (2013)

32. P.M. Garel-Jones, M.R. Harman, T.P. Cutts, Opto-mechanical device having optical element movable by twin flexures, US Patent No. 5594820 (1995)

33. H.-S. Lee, Miniaturization of gradient index lens used in optical components, US Patent No. 6088166 (2000)

34. www.diconfiberoptics.com

35. W.-Z. Li, Q. Shao, Mechanical optical switching device, US Patent No. 6215919 (1999)

36. Y. Fujii, J. Minowa, T. Aoyama, K. Doi, Low loss 4×4 optical matrix switch for fiber-optic communications. Electron. Lett. **15**(14), 427–428 (1979)

37. J. Minowa, Y. Fujii, Y. Nagata, T. Aoyama, K. Doi, Nonblocking 8×8 optical matrix switch for fibre-optic communications. Electron. Lett. **16**(11), 422–423 (1980)

38. J.E. Ford, D.J. DiGiovanni, D.J. Reiley, $1 \times N$ fiber bundle scanning switch, in *Opt. Fiber Commun. Conf.* (OFC'98), San Jose, CA, USA (1998), Techn. Digest, pp. 143–144

39. J.E. Ford, D.J. DiGiovanni, $1 \times N$ fiber bundle scanning switch. IEEE Photonics Technol. Lett. **10**(7), 967–969 (1998)

40. M. Mizukami, M. Makihara, S. Imagaki, K. Sasakura, 200×200 automated optical fiber cross-connect equipment using a fiber-handling robot for optical cabling systems, in *Opt. Fiber Commun. Conf.* (OFC'15), Los Angeles, CA, USA (2015), Techn. Digest, paper OFP5

41. K. Saito, M. Nishimura, T. Yamanishi, H. Koboyashi, T. Katagiri, M. Tachikura, Optical fiber switching device having one of a robot mechanism and an optical fiber length adjustment unit, US Patent No. 5613021 (1995)

42. N. Tamaru, Y. Nishida, T. Kanai, J. Yamaguchi, T. Shoji, Optical fiber cross connection apparatus and method, US Patent No. 5784515 (1998)

43. J. Arol, Z. Ganor, Self-aligning opto-mechanical crossbar switch, US Patent No. 6859575 (2005)

44. K. Goossen, Robotic optical cross-connect, US Patent No. 6307983 (2001)

45. S. Sjolinder, Mechanical optical fibre cross connect, in *Proc. Photon. Switching*, Salt Lake City, UT, USA (1995), paper PFA4

46. B. Pnini, Z. Ganor, R. Cohen, M. Eizenshtat, Optical crossbar switch, US Patent No. 8107779 (2007)

47. www.fiberzone-networks.com

48. A.S. Kewitsch, Large scale, all-fiber optical cross-connect switches for automated patch-panels. J. Lightwave Technol. **27**(15), 3107–3115 (2009)

49. www.telescent.com/tswitch

50. www.emd-performance-materials.com/en/display/lc_materials/lc_phases/lc_phases.html

51. P. Yeh, C. Gu, *Optics of Liquid Crystal Displays*, 2nd edn. Wiley Series in Pure and Applied Optics, vol. 1 (Wiley, Hoboken, 2010)

52. R.A. Soref, Low-cross-talk 2×2 optical switch. Opt. Lett. **6**, 275–277 (1981)

53. J. Prisco, A low-crosstalk liquid crystal optical switch. J. Lightwave Technol. **LT-3**, 37–38 (1985)

54. J. Kondis, B.A. Scott, A. Ranalli, R. Lindquist, Liquid crystals in bulk optics-based DWDM optical switches and spectral equalizers, in *IEEE/LEOS Internat. Conf. Opt. MEMS*, Piscataway, NJ, USA (2001), Techn. Digest, pp. 292–293

55. Meadowlark product catalogue 2009–2010, www.meadowlark.com, pp. 45–62 (2010)

56. An introduction to spatial light modulators. http://laser.physics.sunysb.edu/~melia/SLM_intro.html#4.7

57. Y. Fujii, Low-crosstalk 2×2 optical switch composed of twisted nematic liquid crystal cells. IEEE Photonics Technol. Lett. **5**, 715–718 (1993)

58. G. Lazarev, A. Hermerschmidt, S. Krüger, S. Osten, in *LCOS Spatial Light Modulators: Trends and Applications*, ed. by W. Osten, N. Reingand. Optical Imaging and Metrology: Advanced Technologies (Wiley-VCH, Weinheim, 2012)

59. Holoeye Systems Inc, http://www.holoeyesystems.com/lcos-microdisplays/

60. Beam steering using liquid crystals. White Paper, Boulder Nonlinear Systems (2001)

61. M. Johansson, S. Hard, B. Robertson, I. Manolis, T. Wilkinson, W. Crossland, Adaptive beam steering implemented in a ferroelectric liquid crystal spatial-light-modulator free-space, fiber-optic switch. Appl. Opt. **41**, 4904–4911 (2002)

62. R.E. Wagner, J. Cheng, Electrically controlled optical switch for multimode fiber applications. Appl. Opt. **19**(17), 2921–2925 (1980)

63. R.A. Soref, D.H. McMahon, Total switching of unpolarized fiber light with a four-port electro-optic liquid-crystal device. Opt. Lett. **5**(4), 147–149 (1980)

64. R.A. Soref, Low-cross-talk 2×2 optical switch. Opt. Lett. **6**, 275–277 (1981)

65. Y. Fujii, Low-crosstalk 1×2 optical switch composed of twisted nematic liquid crystal cells. IEEE Photonics Technol. Lett. **5**, 206–208 (1993)

66. N.A. Riza, S. Yuan, Reconfigurable wavelength add-drop filtering based on a Banyan network topology and ferroelectric liquid crystal fiber-optic switches. J. Lightwave Technol. **17**(9), 1575–1584 (1999)

67. N.K. Shankar, J.A. Morris, C.P. Yakymyshyn, C.R. Pollock, A 2×2 fiber optic switch using chiral liquid crystals. IEEE Photonics Technol. Lett. **2**, 147–149 (1990)

68. S. Yuan, N.A. Riza, Low interchannel crosstalk high speed fiber optic $N \times N$ crossconnect switch using polarization optics and ferroelectric liquid crystals, in *Ann. Meeting IEEE Lasers & Electro-Optics Soc.* (LEOS'98), Orlando, FL, USA (1998), Techn. Digest, vol. 2, pp. 415–416

69. P. Gravey, J.L. de Bougrenet de la Tocnaye, B. Fracasso, N. Wolffer, A. Tan, B. Vinouze, M. Razzak, A. Kali, Liquid crystal-based optical space switches for DWDM networks. Ann. Télécommun. **58(9)**, 1378–1400 (2003)

70. P. Berthelé, B. Fracasso, J.L. de Bougrenet de la Tocnaye, Design and characterization of a LC SLM for a polarization-insensitive optical space-switch. Appl. Opt. **37**, 5461–5468 (1998)

71. B. Fracasso, L. Noirie, J.L. de Bougrenet de la Tocnaye, M. Razzak, E. Daniel, Performance assessment of a liquid crystal multichannel photonic space-switch, in *Proc. Photon. Switching*, Monterey, CA, USA (2001), pp. 24–26, paper PThB3

72. N. Wolffer, B. Vinouze, R. Lever, P. Gravey, L. Bramerie, 8×8 holographic liquid crystal switch, in *Proc. 26th Europ. Conf. Opt. Commun.* (ECOC'2000), Munich, Germany (2000), pp. 275–276

73. J. Kelly, Application of liquid crystal technology to telecommunication devices, in *Opt. Fiber Commun. Conf. and Nat. Fiber Opt. Eng. Conf.* (OFC/NFOEC'07), Anaheim, CA, USA (2007), Techn. Digest, paper NThE1

74. www.coadna.com

75. S. Frisken, Advances in liquid crystal on silicon wavelength selective switching, in *Opt. Fiber Commun. Conf. and Nat. Fiber Opt. Eng. Conf.* (OFC/NFOEC'07), Anaheim, CA, USA (2007), Techn. Digest, paper OWV4

76. J.R. Kelly, M. Cui, D. Heineman, H. Washbur, M. Xue, Apparatus and method for optical switching with liquid crystals and birefringent wedges. US Patent 7499608 (2009)

77. S.J. Frisken, G.W. Baxter, H. Zhou, D. Abakoumov, Wavelength selective reconfigurable optical cross-connect. US Patent No. 7787720 B2 (2010)

78. G. Baxter, S. Frisken, D. Abakoumov, H. Zhou, I. Clarke, A. Bartos, S. Poole, Highly programmable wavelength selective switch based on liquid crystal on silicon switching elements, in *Opt. Fiber Commun. Conf.* (OFC'06), Anaheim, CA, USA (2006), Techn. Digest, paper OTuF2

79. www.finisar.com/roadms-wavelength-management/10wsaaxxfll

80. www.hamamatsu.com

81. K. Suzuki, Y. Ikuma, E. Hashimoto, K. Yamaguchi, M. Itoh, T. Takahashi, Ultrahigh port count wavelength selective switch employing waveguide-based I/O frontend, in *Opt. Fiber Commun. Conf.* (OFC'15), Los Angeles, CA, USA (2015), Techn. Digest, paper Tu3A.7

82. T. Han, J. Plumridge, S. Frisken, G. Baxter, LCOS-based matrix switching for 2×4 WSS for fully flexible channel selection, in *Proc. Photon. Switching*, Ajaccio, France (2012), paper Th-S23-005

83. G.I. Papadimitriou, C. Papazoglou, A.S. Pomportsis, Optical switching: switch fabrics, techniques, and architectures. J. Lightwave Technol. **21**(2), 384–405 (2003)

84. Y. Silberberg, P. Perlmutter, J.E. Baran, Digital optical switch. Appl. Phys. Lett. **51**, 1230–1232 (1987)

85. P. DasMahapatra, R. Stabile, K.A. Williams, Multiple input to multiple output switching in an 8×4 optical crosspoint matrix, in *Proc. 40th Europ. Conf. Opt. Commun.* (ECOC'14), Cannes, France (2014), paper P.4.18

86. M.R. Watts, W.A. Zortman, D.C. Trotter, R.W. Young, A.L. Lentine, Vertical junction silicon microdisk modulators and switches. Opt. Express **19**(22), 21989–22003 (2011)

87. V.R. Almeida, C.A. Barrios, R.R. Panepucci, M. Lipson, All-optical control of light on a silicon chip. Nature **431**, 1081–1084 (2004)

88. A.S. Khope, A.A. Saleh, J.E. Bowers, R.C. Alferness, Elastic WDM crossbar switch for data centers, in *Proc. IEEE Opt. Interconn. Conf.* (OI), San Diego, CA, USA (2016), paper TuP7

89. G. Singh, R.P. Yadav, V. Janyani, Ti indiffused Lithium Niobate (Ti: $LiNbO_3$) Mach-Zehnder interferometer all optical switches: a review, in *New Advanced Technologies*, ed. by A.

Lazinica (InTech, 2010). www.intechopen.com. Chap. 2. ISBN 978-953-307-067-4

90. N. Agrawal, C.M. Weinert, H.-J. Ehrke, G.G. Mekonnen, D. Franke, C. Bornholdt, R. Langenhorst, Fast 2×2 Mach-Zehnder optical space switches using InGaAsP–InP multi quantum-well structures. IEEE Photonics Technol. Lett. **7**(6), 644–645 (1995)

91. D.H. Yoon, W.S. Yang, J.M. Kim, H.D. Yoon, Fabrication and properties of a 4×4 LiNbO$_3$ optical matix switch. Mater. Trans. **43**(5), 1061–1064 (2002)

92. E.J. Murphy, C.T. Kemmerer, D.T. Moser, M.R. Serbin, J.E. Watson, P.L. Stoddard, Uniform 8×8 lithium niobate switch arrays. J. Lightwave Technol. **13**(5), 967–970 (1995)

93. H. Nishinoto, M. Iwasaki, S. Suzuki, M. Kondo, Polarization independent LiNbO$_3$ 8×8 matrix switch. IEEE Photonics Technol. Lett. **2**(9), 634–636 (1990)

94. Eospace Inc, Technical specifications of custom high-speed lithium niobate electro-optic switches. www.eospace.com

95. A.C. O'Donnell, Polarisation independent 1×16 and 1×32 lithium niobate optical switch matrices. Electron. Lett. **27**(25), 2349–2350 (1991)

96. H. Okayama, M. Kawahara, Ti: LiNbO$_3$ digital optical switch matrices. Electron. Lett. **29**(9), 765–766 (1993)

97. R. Krähenbühl, M.M. Howerton, J. Dubinger, A.S. Greenblatt, Performance and modeling of advanced Ti: LiNbO$_3$ digital optical switches. J. Lightwave Technol. **20**(1), 92–99 (2002)

98. M. Iodice, G. Mazzi, L. Sirleto, Thermo-optical static and dynamic analysis of a digital optical switch based on amorphous silicon waveguide. Opt. Express **14**(12), 5266–5278 (2006)

99. R.A. Soref, The past, present and future of silicon photonics. IEEE J. Sel. Top. Quantum Electron. **12**, 1678–1687 (2006)

100. L.C. Kimerling, D. Ahn, A.B. Apsel, M. Beals, D. Carothers, Y.K. Chen, T. Conway, D.M. Gill, M. Grove, C.Y. Hong, M. Lipson, J. Liu, J. Michel, D. Pan, S.S. Patel, A.T. Pomerene, M. Rasras, D.K. Sparacin, K.Y. Tu, A.E. White, C.W. Wong, Electronic-photonic integrated circuits on the CMOS platform. Proc. SPIE **6125**, 6–15 (2006)

101. B. Jalali, M. Paniccia, G. Reed, Silicon photonics. IEEE Microw. Mag. **7**, 56–68 (2006)

102. Q. Huang, X. Zhang, J. Xia, J. Yu, Systematic investigation of silicon digital 1×2 electro-optic switch based on a microdisk resonator through carrier injection. Appl. Phys. B **105**(2), 353–361 (2011)

103. L. Liu, G. Roelkens, T. Spuesens, R. Soref, P. Regreny, D. Van Thourhout, R. Baets, Low-power electro-optical switch based on a III–V microdisk cavity on a silicon-on-insulator circuit, in *Optoelectronic Materials and Devices IV*, Shanghai, China (2009), Proc. SPIE **7631**, 7631 0P (2009)

104. A. Biberman, H.L.R. Lira, K. Padmaraju, N. Ophir, M. Lipson, K. Bergman, Broadband CMOS-compatible silicon photonic electro-optic switch for photonic networks-on-chip, in *Conf. Lasers Electro-Opt.* (CLEO/QELS 2010), San Jose, CA, USA (2010), Techn. Digest, paper CPDA11

105. J. van Campenhout, W.M. Green, S. Assefa, Y.A. Vlasov, Low-power, 2×2 silicon electro-optic switch with 110-nm bandwidth for broadband reconfigurable optical networks. Opt. Express **17**, 24020–24029 (2009)

106. P. Dong, S. Liao, H. Liang, R. Shafiiha, D. Feng, G. Li, X. Zheng, A.V. Krishnamoorthy, M. Asghari, High-speed and broadband electro-optic silicon switch with submilliwatt switching power, in *Opt. Fiber Commun. and Nat. Fiber Opt. Eng. Conf.* (OFC/NFOEC'11), Los Angeles, CA, USA (2011), Techn. Digest, paper OWZ4

107. W.M.J. Green, M. Yang, S. Assefa, J.V. Campenhout, B.G. Lee, C.V. Jahnes, F.E. Doany, C.L. Schow, J.A. Kash, Y.A. Vlasov, Silicon electro-optic 4×4 non-blocking switch array for on-chip photonic networks, in *Opt. Fiber Commun. and Nat. Fiber Opt. Eng. Conf.* (OFC/NFOEC'11), Los Angeles, CA, USA (2011), Techn. Digest, paper OThM1

108. J. Xing, P. Zhou, Y. Gong, Z. Li, M. Tan, Y. Yu, J. Yu, Nonblocking 4×4 silicon electro-optic switch matrix with low power consumption. IEEE Photonics Technol. Lett. **27**(13), 1434–1436 (2015)

109. K. Okamoto, Planar lightwave circuits (PLC's), in *Photonic Networks*, ed. by G. Prati (Springer, London, 1997), pp. 118–132

110. A. Himeno, K. Kato, T. Miya, Silica-based planar lightwave circuits. IEEE J. Sel. Top. Quantum Electron. **4**(6), 913–924 (1998)

111. T. Goh, M. Yasu, K. Hattori, A. Himeno, M. Okuno, Y. Ohmori, Low loss and high extinction ratio strictly nonblocking 16×16 thermooptic matrix switch on 6-in wafer using silica-based planar lightwave circuit technology. J. Lightwave Technol. **19**(3), 371–379 (2001)

112. T. Goh, A. Himeno, M. Okuno, H. Takahashi, K. Hattori, High-extinction ratio and low-loss silica-based 8×8 strictly nonblocking thermooptic matrix switch. J. Lightwave Technol. **17**(7), 1192–1199 (1999)

113. T. Goh, A. Himeno, M. Okuno, H. Takahashi, K. Hattori, High extinction ratio and low loss silica-based 8×8 thermooptic matrix switch. IEEE Photonics Technol. Lett. **10**, 358–360 (1998)

114. T. Goh, M. Yasu, K. Hattori, A. Himeno, Y. Ohmori, Low loss and high extinction ratio silica-based strictly nonblocking 16×16 thermooptic matrix switch. IEEE Photonics Technol. Lett. **10**, 810–812 (1998)

115. T. Watanabe, T. Goh, M. Okuno, S. Sohma, T. Shibata, M. Itoh, M. Kobayashi, M. Ishii, A. Sugita, Y. Hibino, Silica-based PLC 1×128 thermo-optic switch, in *Proc. 27th Europ. Conf. Opt. Commun.* (ECOC'01), Amsterdam, The Netherlands (2001), pp. 134–135, paper Tu.L.1.2

116. M. Okuno, N. Takato, T. Kitoh, A. Sugita, Silica-based thermooptic switches. NTT Rev. **7**, 57–63 (1995)

117. T. Nishi, T. Yamamoto, S. Kuroyanagi, A polarization-controlled free-space photonic switch based on a PI-LOSS switch. IEEE Photonics Technol. Lett. **5**, 1104–1106 (1993)

118. www.ntt-electronics.com/en/products/photonics/nxn_n_o_m_s.html

119. S. Sohma, T. Watanabe, N. Ooba, M. Itoh, T. Shibata, H. Takahashi, Silica-based PLC type 32×32 optical matrix switch, in *Proc. 32nd Europ. Conf. Opt. Commun.* (ECOC'06), Cannes, France (2006), paper OThV4

120. K. Watanabe, Y. Hashizume, Y. Nasu, M. Kohtoku, M. Itoh, Y. Inoue, Ultralow power consumption silica-based PLC-VOA/switches. J. Lightwave Technol. **26**(14), 2235–2244 (2008)

121. Enablence Inc, Technical specifications, www.enablence.com

122. L. Eldada, R. Gerhardt, J. Fujita, T. Izuhara, A. Radojevic, D. Pant, F. Wang, C. Xu, Intelligent optical cross-connect subsystem on a chip, in *Opt. Fiber Commun. Conf.* (OFC'05), Anaheim, CA, USA (2005), Techn. Digest, paper NTuL2. See also: Enablence technical white paper at www.enablence.com

123. E.L.W. Rabbering, J.F.P. van Nunen, L. Eldada, Polymeric 16×16 digital optical switch matrix, in *Proc. 27th Europ. Conf. Opt. Commun.* (ECOC'01), Amsterdam, The Netherlands (2001), paper PD.B.1.6

124. L. Eldada, R. Norwood, R. Blomquist, L.W. Shacklette, M.J. McFarland, Thermo-optically active polymeric photonic components, in *Opt. Fiber Commun. Conf.* (OFC'2000), Baltimore, MD, USA (2000), Techn. Digest, vol. 2, pp. 124–126

125. J. Fujita, T. Izuhara, A. Radojevic, R. Gerhard, L. Eldada, Ultrahigh index contrast planar polymeric strictly non-blocking 1024×1024 cross-connect switch matrix, in *Integr. Photon. Res.* (IPR), San Francisco, CA, USA (2004), Techn. Digest, paper IThC3

126. T. Tsuchizawa, K. Yamada, H. Fukuda, T. Watanabe, S. Uchiyama, S. Itabashi, Low-loss Si wire waveguides and their application to thermooptic switches. Jpn. J. Appl. Phys. **45**(8B), 6658–6662 (2006)

127. K. Watanabe, R. Kasahara, Y. Hashizume, Extremely-low-power-consumption thermo-optic switch with silicon-silica hybrid structure. NTT Tech. Rev. **8**(2), 1–5 (2010)

128. K. Tanizawa, K. Suzuki, M. Toyama, M. Ohtsuka, N. Yokoyama, K. Matsumaro, M. Seki, K. Koshino, T. Sugaya, S. Suda, G. Cong, T. Kimura, K. Ikeda, S. Namiki, H. Kawashima, Ultracompact 32×32 strictly-non-blocking Si wire optical switch with fan-out LGA interposer. Opt. Express **23**(13), 17599–17606 (2015)

129. K. Tanizawa, K. Suzuki, M. Toyama, M. Ohtsuka, N. Yokoyama, K. Matsumaro, M. Seki, K. Koshino, T. Sugaya, S. Suda, G. Cong, T. Kimura, K. Ikeda, S. Namiki, H. Kawashima, 32×32 strictly non-blocking Si-wire optical switch on ultra-small die of 11×25 mm^2, in

Opt. Fiber Commun. Conf. (OFC'15), Los Angeles, CA, USA (2015), Techn. Digest, paper M2B.5

130. S. Nakamura, S. Takahashi, M. Sakauchi, T. Hino, M. Yu, G. Lo, Wavelength selective switching with one-chip silicon photonic circuit including 8 × 8 matrix switch, in *Opt. Fiber Commun. Conf. and Nat. Fiber Opt. Eng. Conf.* (OFC/NFOEC'11), Los Angeles, CA, USA (2011), Techn. Digest, paper OTuM2

131. L. Chen, Y.K. Chen, Compact, low-loss and low-power 8 × 8 broadband silicon optical switch. Opt. Express **20**(17), 18977–18985 (2012)

132. K. Suzuki, K. Tanizawa, T. Matsukawa, G. Cong, S.-H. Kim, S. Suda, M. Ohno, T. Chiba, H. Tadokoro, M. Yanagihara, Y. Igarashi, M. Masahara, S. Namiki, H. Kawashima, Ultra-compact 8 × 8 strictly-nonblocking Si-wire PILOSS switch. Opt. Express **22**(4), 3887–3894 (2014)

133. K. Suzuki, G. Cong, K. Tanizawa, S.-H. Kim, K. Ikeda, S. Namiki, H. Kawashima, Ultra-high-extinction ratio 2 × 2 silicon optical switch with variable splitter. Opt. Express **23**, 9086–9092 (2015)

134. C.R. Doerr, L.W. Stulz, D.S. Levy, M. Cappuzzo, E. Cben, L. Gomez, E. Laskowski, A. Wong-Foy, T. Murphy, Silica-waveguide 1 × 9 wavelength-selective cross connect, in *Opt. Fiber Commun. Conf.* (OFC/IOOC'02), Anaheim, CA, USA (2002), Techn. Digest, PDP FA3

135. T. Watanabe, K. Suzuki, T. Takahashi, Multicast switch technology that enhances ROADM operability. NTT Tech. Rev. **12**(1), 1–5 (2014)

136. H. Takahashi, T. Watanabe, M. Okuno, Y. Hibino, T. Goh, Silica waveguide-based optical switches for photonic networks. Techn. Rep. of IEICE **103**(68), 1–6 (2003), CS2003-9 (in Japanese)

137. T. Watanabe, K. Suzuki, T. Goh, K. Hattori, A. Mori, T. Takahashi, T. Sakamoto, K. Morita, S. Sohma, S. Kamei, Compact PLC-based transponder aggregator for colorless and directionless ROADM, in *Opt. Fiber Commun. and Nat. Fiber Opt. Eng. Conf.* (OFC/NFOEC'11), Los Angeles, CA, USA (2011), Techn. Digest, paper OTuD3

138. Neophotonics Inc., www.neophotonics.com/solutions/

139. M.C. Wu, O. Solgaard, J.E. Ford, Optical MEMS for lightwave communication. J. Lightwave Technol. **24**, 4433–4454 (2006)

140. L.Y. Lin, E.L. Goldstein, R.W. Tkach, Free-space micromachined optical switches for optical networking. IEEE J. Sel. Top. Quantum Electron. **5**(1), 4–9 (1999)

141. S.S. Lee, L.Y. Lin, M.C. Wu, Surface-micromachined free-space fibre-optic switches. Electron. Lett. **31**, 1481–1482 (1995)

142. R.S. Muller, K.Y. Lau, Surface-micromachined microoptical elements and systems. Proc. IEEE **86**, 1705–1720 (1998)

143. W. Piyawattanametha, P.R. Patterson, D. Hah, H. Toshiyoshi, M.C. Wu, Surface- and bulk-micromachined two-dimensional scanner driven by angular vertical comb actuators. J. Microelectromech. Syst. **14**, 1329–1338 (2005)

144. P.D. Dobbelaere, K. Falta, L. Fan, S. Gloeckner, S. Patra, Digital MEMS for optical switching. IEEE Commun. Mag. **40**(3), 88–95 (2002)

145. H. Toshiyoshi, H. Fujita, Electrostatic micro torsion mirrors for an optical switch matrix. J. Microelectromech. Syst. **5**, 231–237 (1996)

146. R.A. Miller, Y.C. Tai, G. Xu, J. Bartha, F. Lin, An electromagnetic MEMS 2 × 2 fiber optic bypass switch, in *Proc. Int. Conf. Solid-State Sensors and Actuators*, Chicago, IL, USA (1997), paper 1A4

147. C. Marxer, N.F. de Rooij, Micro-opto-mechanical 2 × 2 switch for single-mode fibers based on plasma-etched silicon mirror and electrostatic actuation. J. Lightwave Technol. **17**(1), 2–6 (1999)

148. R.T. Chen, H. Nguyen, M.C. Wu, A high-speed low-voltage stress induced micromachined 2 × 2 optical switch. IEEE Photonics Technol. Lett. **11**, 1396–1398 (1999)

149. W. Noell, P.A. Clerc, F. Duport, C. Marxer, N. de Rooij, Novel process-insensitive latchable 2 × 2 optical cross connector for single and multimode optical MEMS fiber switches,

in *IEEE/LEOS Internat. Conf. Opt. MEMS*, Piscataway, NJ, USA (2003), Techn. Digest, pp. 49–50

150. L.Y. Lin, E.L. Goldstein, R.W. Tkach, Free-space micromachined optical switches with submillisecond switching time for large-scale optical crossconnects. IEEE Photonics Technol. Lett. **10**, 525–527 (1998)

151. B. Behin, K.Y. Lau, R.S. Muller, Magnetically actuated micromirrors for fiber-optic switching, in *Solid-State Sensor and Actuator Workshop* Cleveland, OH, USA (1998), Techn. Digest, pp. 273–276

152. R.L. Wood, R. Mahadevan, E. Hill, MEMS 2D matrix switch, in *Opt. Fiber Commun. Conf.* (OFC/IOOC'02), Anaheim, CA, USA (2002), Techn. Digest, vol. 1, pp. 91–92

153. L. Fan, S. Gloeckner, P.D. Dobblelaere, S. Patra, D. Reiley, C. King, T. Yeh, J. Gritters, S. Gutierrez, Y. Loke, M. Harburn, R. Chen, E. Kruglick, M. Wu, A. Husain, Digital MEMS switch for planar photonic crossconnects, in *Opt. Fiber Commun. Conf.* (OFC/IOOC'02), Anaheim, CA, USA (2002), Techn. Digest, vol. 1, pp. 93–94

154. P.M. Dobbelaere, S. Gloeckner, S.K. Patra, L. Fan, C. King, K. Falta, Design, manufacture and reliability of 2-D MEMS optical switches. Proc. SPIE **4945**, 39–45 (2003)

155. J.-N. Kuo, G.-B. Lee, W.-F. Pan, A high-speed low-voltage double switch optical crossconnect using stress-induced bending micromirrors. IEEE Photonics Technol. Lett. **16**(9), 2042–2044 (2004)

156. L.-Y. Lin, E.L. Goldstein, R.W. Tkach, On the expandability of free-space micromachined optical cross connects. J. Lightwave Technol. **18**, 482–489 (2000)

157. M.C. Wu, P.R. Patterson, Free-space optical MEMS, in *MEMS: A Practical Guide to Design, Analysis, and Applications*, ed. by J.G. Korvink, O. Paul, (William Andrew, Norwich, 2005), pp. 345–402

158. S. Han, T.J. Seok, N. Quack, B.-W. Yoo, M.C. Wu, Monolithic 50 × 50 MEMS silicon photonic switches with microsecond response time, in *Opt. Fiber Commun. Conf.* (OFC'14), San Francisco, CA, USA (2014), Techn. Digest, paper M2K.2

159. T.J. Seok, N. Quack, S. Han, M.C. Wu, 50 × 50 digital silicon photonic switches with MEMS-actuated adiabatic couplers, in *Opt. Fiber Commun. Conf.* (OFC'15), Los Angeles, CA, USA (2015), Techn. Digest, paper M2B.4

160. M.C. Wu, S. Han, T.J. Seok, N. Quack, Large-port-count MEMS silicon photonics switches, in *Opt. Fiber Commun. Conf.* (OFC'15), Los Angeles, CA, USA (2015), Techn. Digest, paper M2B.3

161. R. Helkey, S. Adams, J. Bowers, T. Davis, O. Jerphagnon, V. Kaman, A. Keating, B. Liu, C. Pusarla, Y. Xu, S. Yuan, X. Zheng, Design of large scale, MEMS based photonic switches. Opt. Photonics News **13**, 40–43 (2002)

162. D.J. Bishop, C.R. Giles, G.P. Austin, The lucent LambdaRouter: MEMS technology of the future here today. IEEE Commun. Mag. **40**(3), 75–79 (2002)

163. V.A. Aksyuk, F. Pardo, D. Carr, D. Greywall, H.B. Chan, M.E. Simon, A. Gasparyan, H. Shea, V. Lifton, C. Bolle, S. Arney, R. Frahm, M. Paczkowski, M. Haueis, R. Ryf, D.T. Neilson, J. Kim, C.R. Giles, D. Bishop, Beam-steering micromirrors for large optical crossconnects. J. Lightwave Technol. **21**, 634–642 (2003)

164. D.T. Neilson, V.A. Aksyuk, S. Arney, N.R. Basavanhally, K.S. Bhalla, D.J. Bishop, B.A. Boie, C.A. Bolle, J.V. Gates, A.M. Gottlieb, J.P. Hickey, N.A. Jackman, P.R. Kolodner, S.K. Korotky, B. Mikkelsen, F. Pardo, G. Raybon, R. Ruel, R.E. Scotti, T.W. Van Blarcum, L. Zhang, C.R. Giles, Fully provisioned 112 × 112 micro-mechanical optical cross connect with 35.8 Tb/s demonstrated capacity, in *Opt. Fiber Commun. Conf.* (OFC'2000), Baltimore, MD, USA (2000), Techn. Digest, vol. 4, pp. 202–204

165. A. Fernandez, B.P. Staker, W.E. Owens, L.P. Muray, J.P. Spallas, W.C. Banyai, Modular MEMS design and fabrication for an 80 × 80 transparent optical cross-connect switch. Proc. SPIE **5604**, 208–217 (2004)

166. Z.J. Yao, N.C. MacDonald, Single crystal silicon supported thin film micromirrors for optical applications. Opt. Eng. **36**(5), 1408–1413 (1997)

167. R.A. Conant, J.T. Nee, K.Y. Lau, R.S. Muller, A flat high frequency scanning micromirror, in *Solid-State Sensor and Actuator Workshop*, Cleveland, OH, USA (2000), Techn. Digest, pp. 6–9

168. J.-L.A. Yeh, J. Hongrui, N.C. Tien, Integrated polysilicon and DRIE bulk silicon micromachining for an electrostatic torsional actuator. J. Microelectromech. Syst. **8**(4), 456–465 (1999)

169. D.S. Greywall, C.-S. Pai, S.-H. Oh, C.-P. Chang, D.M. Marom, P.A. Busch, R.A. Cirelli, J.A. Taylor, F.P. Klemens, T.W. Sorsch, J.E. Bowers, W.-C. Lai, H.T. Soh, Monolithic fringe field-activated crystalline silicon tilting-mirror devices. J. Microelectromech. Syst. **12**(5), 702–707 (2003)

170. D.S. Greywall, P.A. Busch, F. Pardo, D.W. Carr, G. Bogart, H.T. Soh, Crystalline silicon tilting mirrors for optical cross-connect switches. J. Microelectromech. Syst. **12**, 708–712 (2003)

171. O. Tsuboi, Y. Mizuno, N. Kouma, H. Soneda, H. Okuda, S. Ueda, I. Sawaki, F. Yamagishi, Y. Nakamura, A 2-axis comb-driven micromirror array for 3-D MEMS optical switch. Trans. Inst. Electron. Eng. Jpn. **123-E**, 398–402 (2003)

172. J. Kim, D. Christensen, L. Lin, Monolithic 2-D scanning mirror using self-aligned angular vertical comb drives. IEEE Photonics Technol. Lett. **17**(11), 2307–2309 (2005)

173. D. Hah, H.S.-Y. Huang, J.-C. Tsai, J.-C. Toshiyoshi, M.C. Wu, Low-voltage, large-scan angle MEMS analog micromirror arrays with hidden vertical comb-drive actuators. J. Microelectromech. Syst. **13**, 279–289 (2004)

174. N. Kouma, O. Tsuboi, Y. Mizuno, H. Okuda, X. Mi, M. Iwaki, H. Soneda, S. Ueda, I. Sawaki, A multi-step DRIE process for a 128×128 micromirror array, in *IEEE/LEOS Internat. Conf. Opt. MEMS*, Piscataway, NJ, USA (2003), Techn. Digest, pp. 53–54

175. X. Zheng, V. Kaman, S. Yuan, Y. Xu, O. Jerphagnon, A. Keating, R.C. Anderson, H.N. Poulsen, B. Liu, J.R. Schemit, C. Pusarla, R. Helkey, D.J. Blumenthal, J.E. Bowers, Three-dimensional MEMS photonic cross-connect switch design and performance. IEEE J. Sel. Top. Quantum Electron. **9**, 571–578 (2003)

176. J.E. Bowers, Low power 3D MEMS optical switches, in *IEEE/LEOS Internat. Conf. Opt. MEMS Nanophoton.* (OPT MEMS), Clearwater, FL, USA (2009), Techn. Digest, paper ThB1

177. S. Yuan, C. Lee, Scaling optical switches to 100 Tb/s capacity, in *Integr. Photon. Res., Silicon Nanophoton. Photonics in Switching*, Monterey, CA, USA (2010), OSA Techn. Digest, paper PWB3

178. www.glimmerglass.com

179. L. Erdmann, D. Efferenn, Technique for monolithic fabrication of silicon microlenses with selectable rim angles. Opt. Eng. **36**(4), 1094–1098 (1997)

180. J. Kim, A.R. Paparian, R.E. Frahm, J.V. Gates, Performance of large scale MEMS-based optical crossconnect switches, in *15th Ann. Meeting IEEE Lasers & Electro-Optics Soc.* (IEEE/LEOS), Glasgow, Scotland, UK (2002), Techn. Digest, vol. 2, pp. 411–412

181. R. Ryf, J. Kim, J.P. Hickey, A. Gnauck, D. Carr, F. Pardo, C. Bolle, R. Frahm, N. Basavanhally, C. Yoh, D. Ramsey, R. Boie, R. George, J. Kraus, C. Lichtenwalner, R. Papazian, J. Gates, H.R. Shea, A. Gasparyan, V. Muratov, J.E. Griffith, J.A. Prybyla, S. Goyal, C.D. White, M.T. Lin, R. Ruel, C. Nijander, S. Arney, D.T. Neilson, D.J. Bishop, P. Kolodner, S. Pau, C.J. Nuzman, A. Weis, B. Kumar, D. Lieuwen, V. Aksyuk, D.S. Greywall, T.C. Lee, H.T. Soh, W.M. Mansfield, S. Jin, W.Y. Lai, H.A. Huggins, D.L. Barr, R.A. Cirelli, G.R. Bogart, K. Teffeau, R. Vella, H. Mavoori, A. Ramirez, N.A. Ciampa, F.P. Klemens, M.D. Morris, T. Boone, J.Q. Liu, J.M. Rosamilia, C.R. Giles, 1296-port MEMS transparent optical crossconnect with 2.07 petabit/s switch capacity, in *Opt. Fiber Commun. Conf.* (OFC'01), Anaheim, CA, USA (2001), Techn. Digest, paper PD28-1-3

182. M. Kozhevnikov, N.R. Basavanhally, J.D. Weld, Y.L. Low, P.R. Kolodner, C.A. Bolle, R. Ryf, A.R. Papazian, A. Olkhovets, J. Kim, D.T. Neilson, V.A. Aksyuk, J.V. Gates, Compact 64×64 micromechanical optical cross-connect. IEEE Photonics Technol. Lett. **15**(7), 993–995 (2003)

183. A. Olkhovets, P. Phanaphat, C. Nuzman, D.J. Shin, C. Lichtenwalner, M. Kozhevnikov, J. Kim, Performance of an optical switch based on 3-D MEMS crossconnect. IEEE Photonics Technol. Lett. **16**(3), 780–782 (2004)

184. V.A. Aksyuk, S. Arney, N.R. Basavanhally, D.J. Bishop, C.A. Bolle, C.C. Chang, R. Frahm, A. Gasparyan, J.V. Gates, R. George, C.R. Giles, J. Kim, P.R. Kolodner, T.M. Lee, D.T. Neilson, C. Nijander, C.J. Nuzman, M. Paczkowski, A.R. Papazian, F. Pardo, D.A. Ramsey, R. Ryf, R.E. Scotti, H. Shea, M.E. Simon, 238×238 micromechanical optical cross connect. IEEE Photonics Technol. Lett. **15**, 587–589 (2003)

185. D.T. Neilson, R. Frahm, P. Kolodner, C.A. Bolle, R. Ryf, J. Kim, A.R. Papazian, C.J. Nuzman, A. Gasparyan, N.R. Basavanhally, V.A. Aksyuk, J.V. Gates, 256×256 port optical crossconnect subsystem. J. Lightwave Technol. **22**, 1499–1509 (2004)

186. J. Kim, C.J. Nuzman, B. Kumar, D.F. Lieuwen, J.S. Kraus, A. Weiss, C.P. Lichtenwalner, A.R. Papazian, R.E. Frahm, N.R. Basavanhally, D.A. Ramsey, V.A. Aksyuk, F. Pardo, M.E. Simon, V. Lifton, H.B. Chan, M. Haueis, A. Gasparyan, H.R. Shea, S. Arney, C.A. Bolle, P.R. Kolodner, R. Ryf, D.T. Neilson, J.V. Gates, 1100×1100 port MEMS-based optical crossconnect with 4-dB maximum loss. IEEE Photonics Technol. Lett. **15**(11), 1537–1539 (2003)

187. M. Kozhevnikov, R. Ryf, D.T. Neilson, P. Kolodner, C.A. Bolle, A.R. Papazian, J. Kim, J.V. Gates, Micromechanical optical crossconnect with 4-F relay imaging optics. IEEE Photonics Technol. Lett. **16**(1), 275–277 (2004)

188. Y. Mizuno, O. Tsuboi, N. Kouma, H. Soneda, H. Okuda, Y. Nakamura, S. Ueda, I. Sawaki, F. Yamagishi, A 2-axis comb-driven micromirror array for 3D MEMS switches, in *IEEE/LEOS Internat. Conf. Opt. MEMS*, Lugano, Switzerland (2002), Techn. Digest, pp. 17–18

189. M. Yano, F. Yamagishi, T. Tsuda, Optical MEMS for photonic switching-compact and stable optical crossconnect switches for simple, fast, and flexible wavelength applications in recent photonic networks. IEEE J. Sel. Top. Quantum Electron. **11**(2), 383–394 (2005)

190. R. Sawada, J. Yamaguchi, E. Higurashi, A. Shimizu, T. Yamamoto, N. Takeuchi, Y. Uenishi, Single Si crystal 1024-ch MEMS mirror based on terraced electrodes and a high-aspect ratio torsion spring for 3-D cross-connect switch, in *Ann. Meeting IEEE Lasers & Electro-Optics Soc.* (LEOS), Piscataway, NJ, USA (2003), Digest Int. Conf. Opt. MEMS, pp. 11–12

191. T. Yamamoto, J. Yamaguchi, N. Takeuchi, A. Shimizu, E. Higurashi, R. Sawada, Y. Uenishi, A three-dimensional MEMS optical switching module having 100 input and 100 output ports. IEEE Photonics Technol. Lett. **15**, 1360–1362 (2003)

192. J. Yamaguchi, T. Sakata, N. Shimoyama, H. Ishii, F. Simokawa, T. Yamamoto, High-yield fabrication methods for MEMS tilt mirror array for optical switch. NTT Tech. Rev. **5**(10), 1–6 (2007)

193. M. Mizukami, J. Yamaguchi, N. Nemoto, Y. Kawajiri, H. Hirata, S. Uchiyama, M. Makihara, T. Sakata, N. Shimoyama, H. Ishii, F. Shimokawa, 128×128 3D-MEMS optical switch module with simultaneous optical paths connection for optical cross-connect systems, in *Proc. Photon. Switching*, Pisa, Italy (2009), pp. 247–248

194. Y. Kawajiri, N. Nemoto, K. Hadama, Y. Ishii, M. Makihara, J. Yamaguchi, T. Yamamoto, 512×512 port 3D MEMS optical switch module with toroidal concave mirror. NTT Tech. Rev. **10**(11), 1–6 (2012)

195. E. Korevaar, Y. Taketomi, T. Barrott, H. Tigli, M. Last, L. Dirvscio, E. Davis, Optical switch module. US Patent No. 7,734,127 (2007)

196. J.I. Dadap, P.B. Chu, I. Brener, C. Pu, C.D. Lee, K. Bergman, N. Bonadeo, T. Chau, M. Chou, R. Doran, R. Gibson, R. Harel, J.J. Johnson, S.S. Lee, S. Park, D.R. Peale, R. Rodriguez, D. Tong, M. Tsai, C. Wu, W. Zhong, E.L. Goldstein, L.Y. Lin, J.A. Walker, Modular MEMS-based optical cross-connect with large port-count optical switch. IEEE Photonics Technol. Lett. **15**, 1773–1775 (2003)

197. P.M. Hagelin, U. Krishnamoorthy, J.P. Heritage, O. Solgaard, Scalable optical cross-connect switch using micromachined mirrors. IEEE Photonics Technol. Lett. **12**, 882–884 (2000)

198. R.R.A. Syms, Scaling laws for MEMS mirror-rotation optical cross connect switches. J. Lightwave Technol. **20**, 1084–1094 (2002)

199. W.M. Mellette, J.E. Ford, Scaling limits of MEMS beam-steering switches for data center networks. J. Lightwave Technol. **33**(15), 3308–3318 (2015)

200. J.E. Ford, J.A. Walker, Dynamic spectral power equalization using micro-opto-mechanics. IEEE Photonics Technol. Lett. **10**, 1440–1442 (1998)

201. H. Venghaus, A. Gladisch, B.F. Joergensen, J.-M. Jouanno, M. Kristensen, R.J. Pedersen, F. Testa, D. Trommer, J.P. Weber, Optical add/drop multiplexers for WDM communication systems, in *Opt. Fiber Commun. Conf.* (OFC'97), Dallas, TX, USA (1997), Techn. Digest, vol. 4, pp. 280–281

202. J.E. Ford, V.A. Aksyuk, D.J. Bishop, J.A. Walker, Wavelength add-drop switching using tilting micromirrors. J. Lightwave Technol. **17**(5), 904–911 (1999)

203. R. Ryf, Y. Su, L. Möller, S. Chandrasekhar, X. Liu, D.T. Neilson, C.R. Giles, Wavelength blocking filter with flexible data rates and channel spacing. J. Lightwave Technol. **23**, 54–60 (2005)

204. D.T. Neilson, H. Tang, D.S. Greywall, N.R. Basavanhally, L. Ko, D.A. Ramsey, J.D. Weld, Y.L. Low, F. Pardo, D.O. Lopez, P. Busch, J. Prybyla, M. Haueis, C.S. Pai, R. Scotti, R. Ryf, Channel equalization and blocking filter utilizing micro electro mechanical mirrors. IEEE J. Sel. Top. Quantum Electron. **10**, 563–569 (2004)

205. N.A. Riza, M.J. Mughal, Broadband optical equalizer using fault-tolerant digital micromirrors. Opt. Express **11**, 1559–1565 (2003)

206. D.M. Marom, D.T. Neilson, D.S. Greywall, C.-S. Pai, N.R. Basavanhally, V.A. Aksyuk, D.O. López, F. Pardo, M.E. Simon, Y. Low, P. Kolodner, C.A. Bolle, Wavelength-selective $1 \times K$ switches using free-space optics and MEMS micromirrors: theory, design, and implementation. J. Lightwave Technol. **23**, 1620–1629 (2005)

207. D.M. Marom, D.T. Neilson, D.S. Greywall, N.R. Basavanhally, P.R. Kolodner, Y.L. Low, C.A. Bolle, S. Chandrasekhar, L. Buhl, S.-H. Oh, C.-S. Pai, K. Werder, H.T. Soh, G.R. Bogart, E. Ferry, F.P. Klemens, K. Teffeau, J.F. Miner, S. Rogers, J.E. Bowers, R.C. Keller, W. Mansfield, Wavelength selective 1×4 switch for 128 WDM channels at 50 GHz spacing, in *Opt. Fiber Commun.* (OFC/IOOC'02), Anaheim, CA, USA (2002), Techn. Digest, pp. 857–859

208. J. Tsai, S.T.-Y. Huang, D. Hah, M.C. Wu, $1 \times N^2$ wavelength selective switch with two cross-scanning one-axis analog micromirror arrays in a 4-f optical system. J. Lightwave Technol. **24**(2), 897–903 (2006)

209. J. Tsai, S. Huang, D. Hah, H. Toshiyoshi, M.C. Wu, Open-loop operation of MEMS-based $1 \times N$ wavelength-selective switch with long-term stability and repeatability. IEEE Photonics Technol. Lett. **16**, 1041–1043 (2004)

210. J. Tsai, M.C. Wu, A high port-count wavelength-selective switch using a large scan-angle, high fill-factor, two-axis MEMS scanner array. IEEE Photonics Technol. Lett. **18**(13), 1439–1441 (2006)

211. J.-C. Tsai, L. Fan, C.-H. Chi, D. Hah, M.C. Wu, A large port-count 1×32 wavelength-selective switch using a large scan-angle, high fill factor, two-axis analog micromirror array, in *Proc. 30th Europ. Conf. Opt. Commun.* (ECOC'04), Stockholm, Sweden (2004), vol. 2, pp. 152–153

212. www.lumentum.com/en/products/1x9-100-ghz-wss-mini

213. Y. Ishii, K. Hadama, J. Yamaguchi, Y. Kawajiri, E. Hashimoto, T. Matsuura, F. Shimokawa, MEMS-based 1×43 wavelength-selective switch with flat passband, in *Proc. 35th Europ. Conf. Opt. Commun.* (ECOC'09), Vienna, Austria (2009), PDP, session 1

214. W.P. Taylor, J.D. Brazzle, A.B. Osenar, C.J. Corcoran, I.H. Jafri, D. Keating, G. Kirkos, M. Lockwood, A. Pareek, J.J. Bernstein, A high fill factor linear mirror array for a wavelength selective switch. J. Micromech. Microeng. **14**, 147–152 (2004)

215. D.T. Fuchs, C.R. Doerr, V.A. Aksyuk, M.E. Simon, L.W. Stulz, S. Chandrasekhar, L.L. Buhl, M. Cappuzzo, L. Gomez, A. Wong-Foy, E. Laskowski, E. Chen, R. Pafchek, A hybrid MEMS-waveguide wavelength selective cross connect. IEEE Photonics Technol. Lett. **16**, 99–101 (2004)

216. R. Ryf, P. Bernasconi, P. Kolodner, J. Kim, J.P. Hickey, D. Carr, F. Pardo, C. Bolle, R. Frahm, N. Basavanhally, C. Yoh, D. Ramsey, R. George, J. Kraus, C. Lichtenwalner, R. Papazian, J. Gates, H.R. Shea, A. Gasparyan, V. Muratov, J.E. Griffith, J.A. Prybyla, S. Goyal, C.D. White, M.T. Lin, R. Ruel, C. Nijander, S. Arney, D.T. Neilson, D.J. Bishop, S. Pau, C. Nuzman, A. Weis, B. Kumar, D. Lieuwen, V. Aksyuk, D.S. Greywall, T.C. Lee, H.T. Soh, W.M. Mansfield, S. Jin, W.Y. Lai, H.A. Huggins, D.L. Barr, R.A. Cirelli, G.R. Bogart, K. Teffeau, R. Vella, H. Mavoori, A. Ramirez, N.A. Ciampa, F.P. Klemens, M.D. Morris, T. Boone, J.Q. Liu, J.M. Rosamilia, C.R. Giles, Scalable wavelength-selective crossconnect switch based on MEMS and planar waveguides, in *Proc. 27th Europ. Conf. Opt. Commun.* (ECOC'01), Amsterdam, The Netherlands (2001), vol. 6, PDP, pp. 76–77

217. S. Yuan, N. Madamopoulos, R. Helkey, V. Kaman, J. Klingshirn, J. Bowers, Fully integrated $N \times N$ MEMS wavelength selective switch with 100% colorless add-drop ports, in *Opt. Fiber Commun. and Nat. Fiber Opt. Eng. Conf.* (OFC/NFOEC'08), San Diego, CA, USA (2008), Techn. Digest, paper OWC2

218. K. Sorimoto, H. Uetsuka, M. Tachikura, H. Kawashima, M. Mori, T. Hasama, H. Ishikawa, N.A. Idris, H. Tsuda, Compact 5×5 wavelength-selective cross connect using integrated 2-D MEMS mirror arrays, in *18th Microopt. Conf.* (MOC'13), Tokyo, Japan (2013), Techn. Digest, pp. 55–57

219. C.-H. Chi, J.-C. Tsai, D. Hah, S. Mathai, M.-C.M. Lee, M.C. Wu, Silicon-based monolithic 4×4 wavelength-selective cross connect with on-chip micromirrors, in *Opt. Fiber Commun. and Nat. Fiber Opt. Eng. Conf.* (OFC/NFOEC'06), San Francisco, CA, USA (2014), Techn. Digest, paper OTuF

220. V. Kaman, X. Zheng, S. Yuan, J. Klingshirn, C. Pusarla, R.J. Helkey, O. Jerphagnon, J.E. Bowers, A 32×10 Gb/s DWDM metropolitan network demonstration using wavelength-selective photonic crossconnects and narrow-band EDFAs. IEEE Photonics Technol. Lett. **17**, 1977–1979 (2005)

221. www.polatis.com

222. A.N. Dames, J.H. James, Optical fiber switching assembly. US patent No. US 7,106,925 B2 (2006)

223. A.N. Dames, Piezo-electric actuator, US Patent No. US 7,026,745 B2 (2006)

224. A.N. Dames, Beam steering arrangement and optical switches. US Patent No. US 7,095,915 (2006)

Shifu Yuan received the B.S. degree in Applied Physics, M.S., and Ph.D. degrees in Optics, all from the Harbin Institute of Technology, Harbin, China in 1988, 1991, and 1994, respectively. In 1994, he joined the Department of Precision Instruments, Tsinghua University, Beijing China, as a post-doctoral research associate and then an Associate Professor, where he had been engaged in the research and development of photonic information processing and optical image processing and recognition. From 1996 to 1998, he was a post-doctoral research associate with CREOL/School of Optics, University of Central Florida, where he was engaged in the research and development of liquid crystal based optical switch, fiber optics and photonic delay line. In 1998, He joined Chorum Technologies, Richardson, TX, working on liquid crystal based optical switches and birefringent crystal based optical interleavers. In 1999, he joined Corning Inc, Corning, New York, where he had been involved in the research and development of optical networking architectures and applications of wavelength selective switch. In 2000, he joined CALIENT Technologies as a Sr. Optical Engineer and since 2010, he has been the Chief Technology Officer of Optical Technologies at CALIENT. He had been leading the technical team at CALIENT in development of large scale 3-D MEMS optical switches and bringing the largest port count optical switch from design to high volume production.

John E. Bowers holds the Fred Kavli Chair in Nanotechnology, and is the Director of the Institute for Energy Efficiency and a Professor in the Departments of Materials and Electrical and Computer Engineering at UCSB. He is a cofounder of Aurrion, Aerius Photonics and Calient Networks. Dr.

Bowers received his M.S. and Ph.D. degrees from Stanford University and worked for AT&T Bell Laboratories and Honeywell before joining UC Santa Barbara. Dr. Bowers is a member of the National Academy of Engineering, a fellow of the IEEE, OSA and the American Physical Society, and a recipient of the OSA Tyndal Award, the OSA Holonyak Prize, the IEEE LEOS William Streifer Award and the South Coast Business and Technology Entrepreneur of the Year Award. He has published eight book chapters, 600 journal papers, 900 conference papers and has received 54 patents. He and coworkers received the EE Times Annual Creativity in Electronics (ACE) Award for Most Promising Technology for the hybrid silicon laser in 2007.